2020-02-06

Geomorphic response to differential uplift: river long profiles and knickpoints from Guadalcanal and Makira (Solomon Islands)

Boulton, Sarah

10.3389/feart.2020.00010
Frontiers in Earth Science
Frontiers Media SA

Geomorphic response to differential uplift: river long profiles and knickpoints from Guadalcanal and Makira (Solomon Islands)

Sarah J. Boulton[1*]

[1]University of Plymouth, United Kingdom

Submitted to Journal:
Frontiers in Earth Science

Specialty Section:
Geohazards and Georisks

Article type:
Original Research Article

Manuscript ID:
490015

Received on:
06 Aug 2019

Revised on:
07 Jan 2020

Frontiers website link:
www.frontiersin.org

Conflict of interest statement

The authors declare that the research was conducted in the absence of any commercial or financial relationships that could be construed as a potential conflict of interest

Author contribution statement

I undertook all aspects of the research project.

Keywords

Knickpoints, River geomorphology, Solomon Islands, uplift, Landscape response

Abstract

Word count: 350

Knickpoints have long been recognised as key geomorphic features that can be used to reveal the landscape evolution of a region. In particular, mobile knickpoints resulting from relative base-level fall record a landscape in the process of change and can encode information about the timing and rate of landscape response. Here, digital elevation model analysis is undertaken to; a) identify topographic lineaments related to active faulting, and b) extract geomorphic metrics and document associated knickpoints for rivers on Guadalcanal and Makira (San Cristobal) part of the Solomon Island chain. These islands have been experiencing uplift of up to 2 mm/yr since at least the mid Holocene on the upper (Pacific) plate of the San Cristobal Trench of the Solomon Island Forearc. For Guadalcanal, 23 out of 53 studied rivers exhibit slope-break knickpoints, characteristic of base-level fall, and 27 new topographic lineaments with ~E-W orientation are identified. By contrast, on Makira 14 of 41 studied rivers have slope-break knickpoints, where the rivers are steeper below the knickpoint than above. In addition, 76 new lineaments are inferred, trending NE-SW and likely to be extensional faults. For both Guadalcanal and Makira there is a good correlation between knickpoint elevation/catchment area and distance upstream from the sea, and a weak correlation between relief and knickpoint elevation. There are no clear relationships between the knickpoints and the new topographic lineaments. These data indicate that both islands are undergoing active river incision caused by regional tectonic uplift along an active subduction zone. On Makira, river steepness (ksn) scales with uplift, and K, coefficient of erosion, is in the range 1 x 10-5 – 7 x 10-6 m0.1yr-1, while K can be estimated as 1 x 10-5 – 5 x 10-8 m0.1yr-1 for Guadalcanal. Calculation of K for steady-state rivers demonstrates a rock strength control on the fluvial response and highlights the importance of lithology on river evolution. Furthermore, the distinct landscape response of the two islands supports the hypothesis that there are different arc segments present along the Solomon Arc and suggests that the Holocene uplift rates for Guadalcanal may not be representative of long-term uplift.

Contribution to the field

River profile analysis to investigate active tectonics has become a commonly applied method in the last two decades. However, the majority of studies focus on mountain ranges often in arid/semi-arid/Mediterranean climates. Fewer studies have investigated the landscape response to uplift in tropical climates. Here, this research gap is addressed using the islands of Guadacanal and Makira, as they have a well defined uplift field and known seismic risk, to investigate the fluvial geomorphology of transient river systems under tropical climates.

Funding statement

No extenal funding was received as part of this research

Ethics statements

Studies involving animal subjects
Generated Statement: No animal studies are presented in this manuscript.

Studies involving human subjects
Generated Statement: No human studies are presented in this manuscript.

Inclusion of identifiable human data
Generated Statement: No potentially identifiable human images or data is presented in this study.

Data availability statement

Generated Statement: All datasets generated for this study are included in the manuscript/supplementary files.

Geomorphic response to differential uplift: river long profiles and knickpoints from Guadalcanal and Makira (Solomon Islands)

Sarah J. Boulton[1] *

[1] School of Geography, Earth and Environmental Sciences, University of Plymouth, Drake's Circus, Plymouth, PL4 8AA, U.K.

*** Correspondence:**

sarah.boulton@plymouth.ac.uk

Keywords: Knickpoints, river geomorphology, Solomon Islands, uplift, faults

Abstract

Knickpoints have long been recognised as key geomorphic features that can be used to reveal the landscape evolution of a region. In particular, mobile knickpoints resulting from relative base-level fall record a landscape in the process of change and can encode information about the timing and rate of landscape response. Here, digital elevation model analysis is undertaken to; a) identify topographic lineaments related to active faulting, and b) extract geomorphic metrics and document associated knickpoints for rivers on Guadalcanal and Makira (San Cristobal) part of the Solomon Island chain. These islands have been experiencing uplift of up to 2 mm/yr since at least the mid Holocene on the upper (Pacific) plate of the San Cristobal Trench of the Solomon Island Forearc. For Guadalcanal, 23 out of 53 studied rivers exhibit slope-break knickpoints, characteristic of base-level fall, and 27 new topographic lineaments with ~E-W orientation are identified. By contrast, on Makira 14 of 41 studied rivers have slope-break knickpoints, where the rivers are steeper below the knickpoint than above. In addition, 76 new lineaments are inferred, trending NE-SW and likely to be extensional faults. For both Guadalcanal and Makira there is a good correlation between knickpoint elevation/catchment area and distance upstream from the sea, and a weak correlation between relief

and knickpoint elevation. There are no clear relationships between the knickpoints and the new topographic lineaments. These data indicate that both islands are undergoing active river incision caused by regional tectonic uplift along an active subduction zone. On Makira, river steepness (k_{sn}) scales with uplift, and K, coefficient of erosion, is in the range $1 \times 10^{-5} – 7 \times 10^{-6}$ $m^{0.1}yr^{-1}$, while K can be estimated as $1 \times 10^{-5} – 5 \times 10^{-8}$ $m^{0.1}yr^{-1}$ for Guadalcanal. Calculation of K for steady-state rivers demonstrates a rock strength control on the fluvial response and highlights the importance of lithology on river evolution. Furthermore, the distinct landscape response of the two islands supports the hypothesis that there are different arc segments present along the Solomon Arc and suggests that the Holocene uplift rates for Guadalcanal may not be representative of long-term uplift.

1 Introduction

Research into quantitative landscape evolution has undergone a revolution over the last 40 years, with the advent of high-quality global digital elevation models (DEMs) (Finnegan et al., 2005; Pipaud et al., 2015; Harel et al., 2016;), the development of sophisticated computer models of landscape evolution (van der Beek et al., 2002; Whipple and Tucker, 2002; Sklar and Dietrich, 2006; DiBiase et al., 2010) and advances in geochronology (Gosse and Phillips 2001; Balco et al., 2008). In particular, the study of fluvial geomorphology has been a major focus of the landscape evolution community because bedrock rivers transmit base-level changes to the entire watershed and set the hillslope angle; controlling erosion and sediment deposition (e.g., Snyder et al., 2000; Whipple 2004; DiBiase et al., 2010).

One application of fluvial geomorphic analysis has been the study of regional uplift and faulting, where the location and slip rate of individual active faults can even be determined, through the recognition of features indicative of rivers responding to changing boundary conditions, for example an increase in uplift rate or a fall in relative base-level (e.g., Kirby and Whipple, 2001; Boulton and Whittaker, 2009; Kent et al., 2017). Changing boundary conditions cause a characteristic transient landscape response that has been widely recognised across a range of tectonic and climatic regimes, typified by the formation of incised bedrock channels with a knickpoint at the upstream extent of steepened channels (Wobus et al., 2003; Bishop et al., 2005; Harkins et al., 2007; Boulton and Whittaker, 2009; Haviv et al., 2010; Miller et al., 2012; Kirby and Whipple, 2012; Ortega et al, 2013; Regalla et al., 2013; Ferrier et al., 2013; Miller, 2013; Boulton et al., 2014; Castillo et al., 2017; Kent

et al., 2017). The identification, quantification and analysis of rivers and knickpoints, and other features linked to landscape rejuvenation, routinely utilizes global DEM datasets to investigate regional trends in fluvial geomorphology. Therefore, this remote approach to landscape analysis is especially useful in areas that were previously lacking data owing to either accessibility issues or the subtlety of landscape expression (e.g., Oguchi et al., 2003; Ganas et al., 2005; Marliyani et al., 2016; Menier et al., 2017).

In this study, the tropical islands of Guadalcanal and Makira/San Cristobal, part of the Solomon Islands, are investigated. These islands face considerable hazard and risk from significant seismic activity along the adjacent Australia-Pacific plate boundary. Not only are the islands susceptible to the effects of earthquakes and tsunamis but increased landslide hazard is also common in regions experiencing landscape rejuvenation, because tectonic uplift and river incision causes steepening of hillslopes and increased erosion and mass wasting (Malamud et al., 2004; Ouimet et al., 2007; Gallen et al., 2011; Parker et al., 2015; Bennett et al., 2016; Rao et al., 2017). However, limited research into the geology or geomorphology of the islands has been undertaken in recent years. As a result there is little information available on the potential impact of a range of geological hazards that could affect these islands. As populations in the Global South are some of the most vulnerable to geohazards, the lack of recent research presents a significant research gap.

Furthermore, Holocene uplift data (Chen et al., 2011) exist for the two islands allowing a range of fluvial metrics to be compared to the regional uplift field in a tropical island setting with contrasting bedrock lithology. The availability of independently-determined uplift data allow relationships between river steepness and uplift to be assessed and the coefficient of erosion, K, potentially to be determined. K is one of the most difficult of the landscape metrics to calculate and remains unconstrained in many field studies leading to uncertainties the parametrization of this variable in landscape evolution models (Roy et al., 2016; Forte et al., 2016; Yanites et al., 2017). Therefore, determining the natural variation of K is an important challenge for the landscape evolution community.

Therefore, in this study DEMs are used to undertake landscape analysis for Guadalcanal and Makira in the Solomon Island chain that have well-constrained uplift and subsidence rates (Chen et al., 2011). The landscape analysis is used to: a) identify previously unrecognised active faults; b) determine the controls on fluvial network development; c) investigate the relationship between river steepness and uplift, and d) assess the potential implications for geohazards on the islands.

2 Geological Background

The Solomon Island forearc occupies an 800 km long segment of the Australia-Pacific plate boundary in the southwest Pacific Ocean (Mann et al., 1998; Cowley et al., 2004; Kuo et al., 2016). Formed of a collage of crustal units, the islands are surrounded by deep ocean floor and sit on an uplifted tectonic block (Figure 1). The block is bound by two trench systems: the New Britain–San Cristobal trench (or South Solomon trench system) to the SW and the North Solomon trench to the NE. Today most active subduction occurs along the New Britain-San Cristobal trench with only slight convergence along the North Solomon trench (Mann et al., 1998; Miura et al., 2004; Chen et al., 2011). As with other subduction zones, the Solomon Islands forearc can be divided into segments, with three major tectonic regimes or 'super-segments' determined through differences in plate motion, seismic activity and uplift/subsidence rates (Chen et al., 2011). Guadalcanal – Makira is the southernmost of the three segments (the others being the New Georgia Islands and Bougainville Island) and has been further subdivided into five sub-segments by Chen et al. (2011), based primarily upon different histories of vertical tectonic motions across the region. The convergence direction along this segment is oblique, with the Australian Plate subducting along the San Cristobal Trench at 93 mm/yr (Figure 1). As a consequence, the Guadalcanal – Makira segment can be effected by large megathrust earthquakes along the trench and has experienced a number of Mw > 7.0 earthquakes, including an Mw 7.9 earthquake on the 30th April 1939 (Thirumalai et al., 2015; Kuo et al., 2016). In addition, the region experiences frequent lower magnitude seismicity along the subduction zone interface and in the upper plate (Figure 1).

2.1 Geology of Guadalcanal

Guadalcanal is the largest island in the Solomon Island chain (Figure 2A), ~ 150 km in length and 45 km wide, with the highest topography located along the southern half of the island reaching a maximum of 2335 m above sea level at Mount Popomanaseu. The drainage and topographic divides of the island are offset to the south along much of the island, although in western Guadalcanal the divides are centrally located in the volcanic zone (Petterson et al., 1999; Chen et al., 2011).

Basement rocks are exposed in the south and west of Guadalcanal forming part of the South Solomon MORB (Mid Ocean Ridge Basalt) Terrain (Petterson et al., 1997, 1999). The basement lithology of the terrain is mainly composed of basaltic lavas with interbedded pelagic sediments and cross-cut by a range of intrusive sills and dykes (Hackman, 1980; Ridgway, 1987). Overlying is a cover sequence dating from the Oligocene to the Pleistocene, dominantly composed of basaltic or andesitic lavas and volcaniclastic sediments (Hackman, 1980; Cowley et al., 2004). Pliocene deposits consist of siltstones, mudstones and shales, inter-bedded with sandstones and conglomerates (Petterson et al., 1999). Published maps (D.o.S, 1969) indicate that faulting is predominantly located in the basement rocks with ENE-SWS to NE-SE-trending faults dominant (Figure 2A).

Quaternary to Recent sediments are composed of alluvial deposits, located along the central-north sector of the island, which has raised Pleistocene coralline reef terraces up to 800 m above sea level (Hackman, 1980; Petterson et al., 1999). Estimates of Holocene uplift rates come from the work of Chen et al. (2011), who identified two different sub-segments or uplift zones on Guadalcanal. Coral reefs are submerged at the eastern end of the island, indicating that the area is subsiding. However, to the west Holocene reefs are found at increasing elevations reaching a maximum of 15 m above sea-level suggesting uplift rates of up to 2 mm/yr (Chen et al., 2011)(Figure 2A). Interestingly Chen et al. (2011) postulate the presence of an unidentified offshore active fault owing to the presence of adjacent regions of uplift and subsidence along the southern coast. By contrast, in the western part of the island reefs on the north coast indicate maximum uplift rates of 0.8-0.9 mm/yr (Figure 2A) while much of the southern coast appears to be stable or subsiding at the present time (Chen et al., 2011).

2.2 Geology of Makira

The island of Makira (previously known as San Cristobal) is located to the east of Guadalcanal (Figure 1), and is ~ 140 km long and ~ 40 km wide. The topography is lower than Guadalcanal with a maximum elevation of 1056 m. The highest topography lies in the centre and west of the island, yet the drainage divide is offset to towards the south, whereas the topographic divide is located centrally along island (Chen et al., 2011).

The basement sequence forms the Makira Terrain, a composite Cretaceous-Oligocene MORB with plateau basalts (Petterson, 1999) comprising a sequence of basaltic, doleritic and gabbroic intrusions (Figure 2B). The cover sequence comprises Upper Miocene - Lower Pliocene deposits formed of

various breccias, calcareous sandstones and siltstones with interbedded basaltic sheets and a Quaternary-recent sequence of alluvium, raised reef, beach, and mangrove sediments (Tejada et al., 1996; Tejada, 2002).

Makira is also structurally complex and dominated by block faulting (Petterson et al., 1999). To the east faults mainly strike NNE-SSW; whereas, towards the west, faults strike ESE to NNE (Figure 2B). Petterson et al., (1997) explained these structures as the result of the oblique collision between the Australian and Pacific plates causing transpressive sinistral strike-slip deformation.

Chen et al. (2011) also determined that Makira is composed of two arc sub-segments based upon uplift trends. A significant part of the island is characterised by an uplifting northern coast with uplift rates of ~ 0.3 mm/y (Figure 2B) and a stable or subsiding southern coast. The westernmost part of the island experiences similar rates of uplift but the presence of extensive reefs combined with the gross geomorphology led Chen et al. (2011) to assign this region a different Quaternary uplift history.

2.3 Climate

The Solomon Islands have a warm, humid tropical climate with an annual temperature of ~ 26°C and two seasons; the dry season from May to October and the rainy season from November to April. The average annual rainfall is 2000 - 5000 mm but varies owing to the relative influence of the El Niño-Southern Oscillation (ENSO), the Asian-Australian Monsoon and the Indian Ocean Dipole (e.g., Abram et al., 2009). Palaeoclimate records suggest that the ENSO was active throughout the Holocene but that overall Holocene climates were cooler and dryer than today and ENSO oscillations weaker (Tudhope et al., 2001; Abram et al., 2009).

3 Methods

3.1 Mapping of morphostructural lineaments

Topographic or physiographic lineaments have long been recognised as aligned landforms that can be observed at a range of scales and related to underlying crustal structures such as faults and folds (O'Leary et al., 1976). As availability of low cost and free DEMs have revolutionized the extraction

of fluvial geomorphology, so too have they become ubiquitous in the mapping of landforms at a range of scales (e.g., Onorati et al., 1992; Smith et al., 2001; Smith and Clark, 2005). Here, the ALOS World 3D 30 m DEM was used to manually map topographic lineaments on both islands as this dataset has a higher apparent resolution than the SRTM DEM (Boulton and Stokes, 2018).

Smith and Clark (2005) recommend using a range of visualization methods when developing geomorphic maps, to avoid problems in relief-shading causing directional bias in the resulting dataset. They found that no one visualization technique surpassed the advantages of using two or more complementary methods to delimit lineaments, especially where landforms are subdued. In this study, a combination of relief-shaded DEMs (four layers were used, produced with the Hillshade tool in ArcGIS 10.6 with sun azimuth set at 045°, 135°, 225° and 315°), curvature and slope visualization methods were used to identify natural topographic lineaments. In addition, tectonic geomorphic features such as truncated spurs, triangular facets, offset valleys etc., were identified to focus only on the lineaments that are likely to be caused by active faults. However, based upon the available data, active from inactive faults cannot be conclusively separated and all lineaments would need ground truthing in order to fully identify the type of causative structure and determine the sense of motion and activity level. Infrastructure maps were used to cross-check results and avoid mapping any anthropogenic features.

3.2 River profile analysis

Three broad models describing fluvial erosion have been developed: detachment-limited; transport-limited and hybrid models (e.g., Tucker and Whipple, 2002; Whipple and Tucker, 2002). In detachment-limited systems the steady-state (where erosion equals uplift) river gradient is controlled by the strength of the channel substrate and relative base-level fall; these rivers are characteristically bedrock rivers.

These models of river behaviour predict the relationship between slope, S, and upstream drainage area, A, in the form:

$$S = k_s A^{-\theta} \quad (1)$$

where Θ is the concavity index and k_s the steepness index.

203 Where k_s = (uplift/erosion coefficient)$^{1/n}$ (2)

204 As eq [1] subsumes within k_s the uplift rate of a given area (Eq. 2) this term should vary
205 systematically with uplift at steady state (Whipple and Tucker, 1999; 2002), a conclusion that has
206 been supported by a range of empirical studies (i.e., Snyder et al., 2000; Kirby and Whipple, 2001;
207 Safran et al., 2005; DiBiase et al., 2009; Cyr et al., 2010). The erosion coefficient, K, encompasses
208 several factors including rock strength, channel width and runoff, yet despite recent modelling and
209 empirical studies this variable remains poorly constrained (Snyder et al., 2000; Stock and
210 Montgomery, 1999; Roy et al., 2016; Bernard et al., 2019).

211 In addition, the stream power model predicts that the shape of the river will be concave-up under
212 presumed steady-state conditions (Figure 3A)(Whipple and Tucker, 2002; Kirby et al., 2003).
213 However, where uplift ≠ erosion, the river is no longer in steady-state and non-equilibium
214 geomorphic features (i.e., knickpoints) may develop (Figures 3C and E). Knickpoints are recognised
215 in the field as steeper channel reaches through to waterfalls and have been classified into two end
216 member morphologies: vertical-step and slope-break (Figures 3D and F), based upon their form on
217 slope-area graphs (Haviv et al., 2010).

218 Slope-break knickpoints (Haviv et al., 2010; Kirby and Whipple, 2012) develop in response to a
219 change in the base-level of the system, forcing the fluvial system from one steady state to another.
220 For example, changes in boundary conditions can result from an increase in rock uplift as a result of
221 the initiation of new faults, the increase in slip rate on existing faults, or permanent eustatic sea-level
222 fall (Wobus et al., 2003, 2006; Goldrick and Bishop, 2007; Harkins et al., 2007; Marliyani et al.,
223 2016). The slope-break knickpoint transmits the new base-level to the catchment as a migrating
224 wave through the river system. The horizontal celerity is a function of drainage area, so as the
225 knickpoint travels through the drainage system the celerity decreases as catchment area decreases
226 (Whipple and Tucker, 1999; Crosby & Whipple, 2006). Therefore, within a single catchment the
227 knickpoints will migrate at a rate proportional to drainage area and at any given time will occur at a
228 constant elevation within the landscape assuming that prior to perturbation the landscape was in
229 equilibrium (Crosby & Whipple, 2006). However, differences in knickpoint elevation can be
230 observed as a result of spatial variation in uplift rates along a fault, climatic variations across a study
231 area or where the pre-existing landscape was not in steady-state (Bishop et al., 2005). Where
232 knickpoint dispersal is the result of variations in uplift rate along normal fault arrays, the height of

the knickpoint has been shown to correlate with the slip rate on faults (Boulton and Whittaker 2009; Whittaker and Boulton 2012; Gallen and Wegmann 2017; Kent et al. 2017). This observation means that in regions without independent means to determine uplift rates the transient river profile provides a mechanism by which fault activity can be evaluated.

By contrast vertical-step knickpoints are generally stationary, anchored in space as a result of a discrete change in channel conditions, such as a more resistant bedrock lithology, a debris flow or landslide causing the deviation away from steady state conditions (Phillips and Lutz, 2008; Haviv et al., 2010; Kirby & Whipple, 2012). Vertical-step knickpoints can also mark the position of faults in the landscape where there is marked lithological change across the structure (Whipple 2004; Wobus et al. 2006; Kirby and Whipple 2012; Liu et al., 2019). In general, the significance of vertical-step knickpoints is more relevant to smaller channel-scale heterogeneities rather than regional-scale trends in uplift or sea-level fall.

Longitudinal river profiles were extracted from the SRTM 30 m DEM (Farr et al., 2007; USGS, 2019) using a combination of the Matlab stream profiler tool and the ArcGIS suite of programmes using the ArcHydrology toolbox (Tarboton et al., 1991) to create a hydrologically sound DEM and to extract the river network. Major river systems were extracted that drain the islands of Guadalcanal and Makira where drainage area exceeds 10^5 m^2 (cf. Kirby and Whipple, 2001, 2012). The SRTM DEM is of higher quality than the ASTER DEM for the region, this is in line with observations elsewhere (e.g., Boulton and Stokes, 2018). This analysis was completed before the ALOS World dataset was released, and previous research shows that DEM choice has little effect on the results of river profile analysis (e.g., Wobus et al., 2006; Boulton and Stokes, 2018). Channel slope, S, and upstream drainage area, A, were plotted on SA log-log plots and used to calculate the channel concavity, Θ, and the steepness index, k_s, through slope regression (Figure 3). As the concavity determines k_s, a reference concavity Θ_{ref} (Wobus et al., 2006) is used to calculate the normalized steepness index, k_{sn}. A standard $\Theta_{ref} = 0.45$ is used to be consistent with other studies (e.g., Wobus et al., 2003; 2006; Ouimet et al., 2009; DiBiase et al., 2010; Miller et al., 2012; Cyr et al., 2014) allowing for inter-study comparison.

Knickpoints were identified based upon observed breaks in scaling on the SA plots (Figure 3). On rivers where knickpoints were identified, Θ and k_{sn} were calculated separately for channel reaches above and below the knickpoint(s). Knickpoints were also mapped onto the DEM so that any spatial

relationships between knickpoint locations and lithological boundaries based upon the published map (D.o.S, 1969) or inferred faults from DEM analysis could be identified.

3.3 Uplift rates

Uplift values were interpolated across the two islands using the dated Holocene coral database of Chen et al., (2011). This was achieved in ArcMap using a spline with barriers tool. The spline interpolation technique was chosen as this technique honours the original datapoints (i.e., the output surface passes through the input points) and the barriers to take into account possible discontinuities in the uplift field across proposed arc segments. A disadvantage of this method is that the resultant uplift field is restricted to the x, y extent of the input points.

4 Results

4.1 Guadalcanal lineaments

There are limited structural data available for Guadalcanal, although the published geological map (D.o.S, 1969) includes 69 faults mapped primarily in the igneous basement but also deforming the Pliocene sediments (Figure 4A). The dominant trend of these mapped faults is NE-SW, with secondary fault trends in the SE-NW quadrant. Interestingly, the SE-NW orientated structures have longer mapped traces (up to 50 km) but are less common than the shorter NE-SW trending faults. Both sets of faults can be found across the whole island and there are no clear patterns of cross-cutting relationships suggesting that these two sets of structures could be a conjugate fault system (Figure 4).

Interestingly, many of these previously mapped faults do not have a clear topographic expression. Only 27 lineaments were identified through the topographic analysis of the DEM. The majority of these structures are oriented ESE-WNW, with few lineaments striking NE-SW. In some cases, the traces of the new faults are located close to mapped structures suggesting that these could be the same fault but that errors in location could have resulted in slight mismatches between datasets. For example in the south of the island (Figure 4B and C), a topographic lineament was identified based upon truncated spurs and aligned valleys, with transverse and offset streams. This new lineament is

located in between two previously identified subparallel structures trending ESE-WNW, which have limited topographic expression. These ESE-WNW striking structures appear to be truncated by a cross-cutting N-S lineament with triangular facets forming the western-side of a river valley (Figures 4B and C). Other mapped lineaments are present in this area but do not have clear topographic expression.

4.2 Guadalcanal Rivers

On the island of Guadalcanal, 57 river profiles that drain radially from the central high topography to the coast were extracted from the SRTM 30 m DEM (Figure 5; Table 1). Twenty-five rivers flow to the north, these are in general longer (average length 48.7 km; longest river 13 at 69.95 km) than the 32 rivers that flow southwards (average 16.7 km, longest rivers are rivers 33 and 40 both 33 km long). Of the 57 river profiles extracted, 24 contain one or more knickpoints, while the remaining 33 rivers have river long profiles without any marked discontinuities.

Rivers without knickpoints more commonly flow to the south coast of the island (18 rivers), than to the north (11 rivers). The average concavity (θ) for all rivers across the island is 0.49, with little variation between the southerly flowing rivers ($\theta = 0.46$) and the northerly flowing ones ($\theta = 0.54$). Whereas the steepness index does vary significantly between the south and north from 111.1 to 59.2 $m^{0.9}$, respectively.

By contrast, rivers flowing northwards contain the majority of the knickpoints, where 14 rivers have a single prominent knickpoint, and rivers 1 and 20 have two clear knickpoints. Above the knickpoint (in the river headwaters) the average $\theta = 0.62$ and the steepness index (k_{sn}) = 58.9 $m^{0.9}$; while downstream of the knickpoint, $\theta = 1.4$ and $k_{sn} = 87.9$ $m^{0.9}$. A similar pattern is seen in the 10 rivers containing knickpoints that drain to the south, upstream of the knickpoint $\theta = 0.5$ and $k_{sn} = 71.5$ $m^{0.9}$, while downstream $\theta = 0.8$ and $k_{sn} = 130.7$ $m^{0.9}$. Therefore, there is a consistent pattern of over-steepened ($\theta > 0.8$) rivers downstream of the knickpoint in both the northern and southern rivers, although in general the southern rivers are steeper and shorter than in the north. These rivers show the typical geometry of slope-break knickpoints and the location of mapped knickpoints does not clearly correlate with either mapped geological boundaries or faults.

Where there are two knickpoints observed in the river profiles this observation holds true for the higher knickpoint; whereas, for the lower elevation knickpoint there is a decrease in k_{sn} downstream

across the knickpoint. This knickpoint morphology is more characteristic of vertical-step knickpoints, with spike in the values on the SA plot. These knickpoints will not be considered further as it is likely that such knickpoints are the result of lithological discontinuities.

When analyzing slope-break knickpoint formation and behaviour, the vertical and horizontal components of knickpoint retreat need to be considered. The horizontal knickpoint retreat distance was measured from the coast; in the absence of a clear causative fault, this datum provides a constant reference elevation with which to compare rivers within and across islands. When the upstream distance of the knickpoint is compared to the total drainage area (Figure 6A) of the catchment there is a good ($r^2 = 0.8$) correlation between the two variables with a power law relationship ($L \sim A^{0.56}$), demonstrating that in larger river catchments the knickpoints have migrated further upstream, for example in river 13 with a drainage area of 650 km^2 the knickpoint is 67 km upstream, whereas along river 8 with a catchment area of 45 km^2 this knickpoint is ~ 16 km upstream. This observation is consistent with observations from numerous other studies (e.g., Crosby and Whipple, 2006; Harkins et al., 2007; Miller et al., 2012; Whittaker and Boulton, 2012; Kent et al., 2017) and with theoretical predictions from simple stream power models ($L = A^{0.5}$). A similar scaling relationship is observed between the downstream distance from the drainage divide and the catchment area upstream of the knickpoint (Figure 6B). It is important to note that knickpoints from northwards and southwards flowing rivers plot together and that there is no difference in the scaling relationships of the two groups.

When the relationship between the elevation of the slope-break knickpoints and the catchment areas of their rivers is examined (Figure 6C), to investigate the vertical component of knickpoint migration, there is a weak correlation ($r^2 = 0.3$) between higher elevation knickpoints occurring in larger catchments across the whole island. Similarly, there is a weak relationship ($r^2 = 0.3$) between the knickpoint elevation and the upstream distance of the knickpoint from the mouth of the river at sea-level (Figure 6D). When the upstream distance of knickpoints is compared between the rivers draining to the north and the south, this relationship is slightly strengthened ($r^2 = 0.37$ and 0.44, respectively).

Yet, when the elevation of the knickpoints is considered along the strike of the island there is no clear distinction between the two sets of the knickpoints, with the majority of knickpoints falling in the 200 – 600 m above sea-level range with only six knickpoints found at higher elevations, present in

rivers on both sides of the island (Figure 7). The majority of knickpoints appear to plot close to the average elevation along the island. When the k_{sn} above and below the knickpoint is plotted along the strike of island both sides of the island show a general increase in steepness from the NW to the SE (Figure 8A) from 72 to 180 $m^{0.9}$. While there is a clear separation in k_{sn} values above and below identified knickpoints. It is interesting to note that k_{sn} values from rivers without knickpoints span the whole range of the observed values. In addition, the ratio of k_{sn} change from above to below the knickpoint is fairly constant along the length of the island and there is no clear trend in behaviour (Figure 8B).

When knickpoint elevation and k_{sn} values are compared to the geomorphic relief of the topography it is apparent the both knickpoint height and k_{sn} are higher where the topographic relief is greater (Figure 8C), although there is only a weak correlation ($r^2 = 0.28$) between k_{sn} downstream of knickpoints than between upstream values or overall knickpoint elevation (Figures 8D).

4.3 Makira Lineaments

In comparison to Guadalcanal there are fewer mapped structures on the published map of Makira (D.o.S, 1969), 52 faults (Figure 9A) are shown with almost all located in the basement geology that dominates the island. The published faults are mainly NW-SE and E-W striking structures with minor ~ N-S striking faults.

A significant number of topographic lineaments were identified for Makira, with a total of 76 potential faults identified from the DEM (Figure 9). Many, such as those in the NW of the island (Figures 9 B and C) have strong topographic expression, with changes in elevation, offset topographic features and aligned river systems along the strike of the features. The majority of these topographic lineaments strike NE-SW across the whole island, although structures striking E-W/NW-SE are more common in the western part of the island and could be conjugate structures to the dominant NE-SW striking features. As for Guadalcanal, some lineaments with topographic expression are coincident with previously mapped faults but many are newly recognized here.

4.4 Makira Rivers

The island of Makira is a similar size to Guadalcanal, although fewer large rivers are present on this island. In total 41 rivers were analysed with 26 draining to the north coast and 15 flowing to the south (Figure 10; Table 3). The average length of the rivers is greater for northward than for southward flowing rivers, at 35.7 and 15.3 km, respectively. Nineteen rivers show clear knickpoints along their profile, with 10 draining northwards and only 5 rivers draining to the south exhibiting knickpoints.

The average concavity (θ) for all rivers across the island that do not have knickpoints is 0.57, with some variation between the southerly flowing rivers ($\theta = 0.64$) and the northerly flowing ones ($\theta = 0.5$). Similarly, the steepness index varies between the south and north from 60.2 to 35.7 $m^{0.9}$, respectively, consistent with the southern rivers being steeper than northern rivers. This relationship was also observed on Guadalcanal to the north.

Rivers flowing northwards contain the majority of the knickpoints, where most rivers have a single prominent knickpoint, and rivers 5 and 23 have two clear knickpoints. Above the knickpoint (in the river headwaters) the average $\theta = 0.78$ and $k_{sn} = 28.9$ $m^{0.9}$ and downstream of the knickpoint, $\theta = 1.1$ and $k_{sn} = 50.8$ $m^{0.9}$. A similar pattern is seen in the five rivers containing knickpoints that drain to the south, upstream of the knickpoint $\theta = 0.79$ and $k_{sn} = 26.1$ $m^{0.9}$, while downstream $\theta = 0.8$ and $k_{sn} = 54.8$ $m^{0.9}$. Therefore, there is a consistent pattern of steeper rivers downstream of the knickpoint in both the northern and southern rivers, although in general the concavity of the rivers above and below knickpoints is similar but overall higher than in the rivers without knickpoints. In addition, the location of these knickpoints does not clearly correlate with mapped geological boundaries with the majority of knickpoints falling within the older igneous and volcanic complex. Although some knickpoints do appear to fall close to faults, overall these characteristics are typical of slope-break knickpoints.

When the upstream distance of the knickpoint is compared to the total drainage area (Figure 11A) of the catchment there is a good ($r^2 = 0.7$) correlation between the two variables with a power law relationship ($L \sim A^{0.57}$), demonstrating that in larger river catchments the knickpoints have migrated further upstream. Rivers flowing to the north and south plot in the same field demonstrating a similarity in behaviour across the island. Interestingly this relationship is virtually the same as for Guadalcanal (Figure 6A), although for the Makira the correlation is not quite so strong. The scaling relationship between knickpoint distance from divide and the catchment area above the knickpoint

also shows a strong correlation ($r^2 = 0.96$) consistent with theoretical models of stream power (Figure 11B).

In contrast to Guadalcanal there is no clear relationship between catchment area and k_{sn} (Figure 11C), although in general knickpoint elevation does increase as the distance from the river mouth increases (Figure 11D). This pattern becomes stronger when the knickpoint elevation is considered along the strike of the island (Figure 12). In the northern 60 km of the island, the maximum elevation of the topography is ~ 600 m, while mean elevation is ~ 200 m. The elevations of knickpoints reflect the overall topography ranging from 160 – 380 m in elevation, the majority of the knickpoints fall around the mean elevation of the topography with few sitting high up in the catchments. Whereas, in the central part of the island maximum and mean elevations increase, with maximum elevations reaching > 1000 m. Here knickpoints are mostly high in elevation located near the maximum elevation. Interestingly for the island of Makira there is a clear relationship between the topography and the interpolated uplift rates, with the lower topography found in the north and south of the island correlating with zones of subsidence or low rates of uplift. The inflection points between areas of subsidence and uplift closely correspond to the margins of the topographically higher central part of the island, where uplift rates reach > 0.6 mm/yr (Chen et al., 2011).

When the k_{sn} values are considered along the strike of the island (Figure 13A) a similar pattern is observed, with values above and below the knickpoint generally lower in the north and extreme south, while they are up to two times higher in the south central part of the island. This trend is not as clear in the ratio between steepness index above and below the knickpoint but interestingly k_{sn} ratios are higher in southern catchments than in northern ones (Figure 13B). However, when topographic relief is considered there is only a weak positive trend with knickpoint elevation (Figure 13C). No trend is apparent with relief is compared to k_{sn}, with k_{sn} being rather invariant with respect to relief (Figure 13D).

5 Discussion

5.1 Origin and implications of knickpoints

Slope-break knickpoints have been identified along river systems on both Guadalcanal and Makira. These geomorphic features typically form along bedrock rivers responding to a relative base-level

fall, which causes a transient wave of incision to propagate up through the catchments as the river adjusts to the new boundary conditions. However, what caused the formation of the knickpoints observed on Guadalcanal and Makira? Were knickpoints triggered by eustatic sea-level fall, localized faulting or regional tectonic uplift?

In the Pacific, eustatic sea-level has experienced two periods of significant sea-level fall in the last 140 kyrs. Firstly, at 140 ka the sea-level was ~135 m lower than present, and at the climax of the last glacial (20 Ka; Woodroffe & Horton, 2005). This eustatic fall in base-level has been implicated in the formation of knickpoints described on the Pacific islands of Tahiti (Ye et al., 2013) and Hawaii (Seidl et al., 1994). However, the knickpoints described on these islands are morphologically waterfalls rather than steep fluvial reaches, the majority of rivers are typically < 10 km in length and many have linear river profiles. Furthermore, the knickpoints typically occur near the coast as hanging-valleys. Neither Ye et al. (2013) nor Seidl et al. (1994) classified the observed waterfalls as vertical-step or slope-break but they may be vertical-step in nature. Therefore, the morphology of the eustatic sea-fall generated waterfalls previously recorded on other Pacific Islands is dissimilar to those recognised on Guadalcanal and Makira.

In addition, knickpoints developed as the result of sea-level fall would be expected to have the following characteristics. Firstly, knickpoints would be expected to occur in all rivers, except those that are short so that in the response time of the system the knickpoints would have migrated through the catchment (or the knickpoints would be trapped at a threshold drainage area [c.f., Crosby and Whipple, 2006]). Secondly, knickpoints would have formed at the same time and thus show consistent scaling, and knickpoint elevation within and across catchments should be in a narrow band. Finally, where lithology and climate are similar there should be no variations in k_{sn} or k_{sn} ratio across the island. By contrast, knickpoints forming as a result of a change in the rate of uplift, or potentially a switch from subsidence to uplift, would show along strike variations in the k_{sn} values, as k_{sn} is known to positively scale with uplift (e.g., Snyder et al., 2001). In this scenario, if the uplift affected an entire island or arc segment, all rivers would also be affected. Therefore, the key discriminating factor to determine the likely mechanism of knickpoint formation is the k_{sn} of the river systems.

For the island of Makira, k_{sn} values (Figure 13) show an increase towards the south, with a peak in values at 110 km along strike. This pattern correlates with the inferred uplift rates across the island

(Figure 12), where uplift rates reach a maximum ~ 0.7 mm/yr at 110 km along strike, and is also reflected in the elevation of the knickpoints also reaching maximum heights in the southern half of the island (c.f. Boulton and Whittaker, 2009). When the inferred uplift rate at the mouth of the rivers is plotted against k_{sn} values for steady-state rivers there is a positive, although weak, linear relationship (Figure 14) reflecting these previous observations.

By contrast on the island of Guadalcanal, k_{sn} values along strike are fairly constant (average k_{sn} = 67 $m^{0.9}$) from 0 – 50 km (Figure 7), with an increase in k_{sn} to an average of 100 $m^{0.9}$ in the southern two thirds on the island. Yet, when the uplift values are interpolated from available data the uplift field of the island is also fairly constant at ~ 1 – 0.4 mm/yr but showing an overall decrease to the south. Although, k_{sn} and relief are positively correlated, the topography appears decoupled from the uplift data available and the correlation between k_{sn} and uplift rates is invariant (Figure 14).

There is no clear pattern of knickpoint location upstream of potentially active faults, as would be expected if knickpoints were generated because of changes in motion along individual structures. Indeed, on both islands knickpoints are present along rivers that apparently do not cross faults (either previously published or inferred from DEM analysis carried out in this study). In addition, on both islands knickpoints are more common in the longer northwards flowing rivers than on the southwards flowing rivers, which also tend to be steeper than those flowing to the north. These observations suggest; a) a regional rather than local control on knickpoint formation, and b) that knickpoints may have already completely migrated through the short steep southern rivers implying that the timing of knickpoint formation was longer ago than the response times of the rivers. Some rivers have response times of millions of years, albeit in drier climates (e.g., Italy ~1-2 x 10^6 Myr [Whittaker et al., 2017]), but even in tropical climates response times are likely > 25 Ka (Whipple, 2001).

In summary, although the evidence for Guadalcanal is somewhat equivocal, the patterns of knickpoints and the correlation between k_{sn} and uplift rates for Makira demonstrate that the landscape is transiently responding to regional uplift along the subduction zone as opposed to eustatic sea-level fall. Therefore, this is likely also to be the cause of knickpoints on the nearby island of Guadalcanal. Uplift, and the associated base-level fall can only trigger knickpoint formation and propagation when there is an increase in the uplift rate. A question remains over when and why this increase in uplift might have taken place, but uplift could be linked to variable rates of strain accumulation that has been evidenced elsewhere in the Solomon Arc (Thirumalai et al., 2015).

499

500 **5.2 Uplift dependent channel steepness**

501 It is of note that the fluvial geomorphic responses are distinct given that rates of uplift and climate are
502 similar for the two islands. There is a positive, albeit weak, correlation ($R^2 = 0.4$) between uplift and
503 k_{sn} for rivers without knickpoints for Makira. Whereas, there is no correlation between these variables
504 along river reaches upstream or downstream of knickpoints (Figure 14). On Guadalcanal, there is no
505 clear correlation between inferred uplift and k_{sn} for any river reaches (Figure 14). This dichotomy
506 could be the result of a recording bias, for example the rates derived from uplifted coral reefs of
507 Makira are more representative of long-term uplift rates but on Guadalcanal the uplift recorded by the
508 coral reefs could be representative only of short interseismic strain and are not equal to the longer
509 term rates to which the rivers are responding. This explanation is also consistent with Guadalcanal
510 and Makira being located on two different arc segments and having different uplift histories (Chen et
511 al., 2011).

512 However, the contrast in fluvial response equally could be a result of the more complex bedrock
513 geology of Guadalcanal, compared to Makira that is dominated by basement MORB (Figure 2). The
514 assumption that channel gradient varies linearly with tectonic forcing is only true where K
515 (erodibility coefficient) is uniform across the region (Whipple and Tucker, 1999; Snyder et al., 2000).
516 As K embeds rock strength, regional lithological variability can result in K scaling over several
517 orders of magnitude (Stock and Montgomery, 1999). Therefore, different bedrock geology can
518 explain the contrasting landscape response and the lack of scaling between k_{sn} and uplift (U) on
519 Guadalcanal.

520 Cyr et al. (2010) state that the channel longitudinal profile must be in steady-state so that U as well as
521 K is uniform along the channel to determine K. This condition therefore appears likely to be satisfied
522 for the concave-up rivers on Makira (although the relationship is weak) and explains why there is no
523 correlation between the variables where knickpoints are present, as these rivers are not in steady-
524 state. Furthermore, the linear k_{sn} to U scaling implies that the *n* exponent in Eq. (2) is ~ 1, which is
525 consistent with a range of other studies across a range of climatic zones (i.e., Burbank and Anderson,
526 2001; Wobus et al., 2006; D'Arcy and Whittaker, 2014). Therefore, assuming that U = E in the
527 concave-up rivers, one can derive values of K in the range $1 \times 10^{-5} - 7 \times 10^{-6}$ $m^{0.1}yr^{-1}$ for Makira
528 where uplift is positive using the results of the stream profile analysis and the interpolated uplift field

529 [eq. 2]. K can also be estimated for Guadalcanal using k_{sn} for the rivers without knickpoints,
530 assuming U = E and n = 1, deriving values of K in the range 1 x 10^{-5} – 5 x 10^{-8} $m^{0.1}yr^{-1}$. The spread
531 of values likely reflect a combination of factors that are difficult to quantify given existing data, such
532 as precipitation gradients across the island, variability in channel morphology or local rock strength
533 variations not captured by regional scale mapping. These values are consistent with values reported
534 elsewhere; for example, Stock and Montgomery (1999) reported values in the range of 10^{-2} to10^{-7}
535 $m^{0.2}yr^{-1}$ for a range of rock types across a number of climatic zones. Similarly, Brocard and Van der
536 Beek (2006) determined that for bedrock rivers in the French Alps K = 1.1 - 4.7 x 10^{-5} $m^{0.4}$ yr^{-1} and
537 van der Beek and Bishop (2003) determined that K = 7 x 10^{-7} $m^{0.4}$ yr^{-1} for a river crossing crystalline
538 basement rocks in SE Australia. Therefore, it is likely that the larger range of K parameter values
539 estimated for Guadalcanal reflect the greater variation in bedrock lithologies present on this island
540 compared to Makira, especially the presence of presumably weaker sedimentary rocks (sandstones,
541 siltstones) in addition to the stronger basement lithologies found on both islands (Katz et al., 2000).
542 These data support the hypothesis that rock strength is a key control on landscape evolution in the
543 Solomon Islands.

544

545 **5.3 Geohazard Implications**

546 As demonstrated above the fluvial geomorphology on the islands of Guadalcanal and Makira is
547 transiently responding to a base-level fall that is interpreted as the result of regional uplift modulated
548 by rock strength along this segment of the Solomon Islands Forearc. Although it is well known that
549 this region can be affected by strong (> 7.0 M_w) megathrust earthquakes, this research highlights the
550 landscape vulnerability to the tectonic activity along the subduction zone.

551 Firstly, it is probable that at least some of the mapped faults pose a hitherto unquantified earthquake
552 hazard and warrant further investigation. Although, many of the mapped faults on the islands of
553 Guadalcanal and Makira have no clear expression in the landscape that is identifiable through DEM
554 analysis, it is not clear if these faults are inactive or if high erosion rates and/or vegetation cover
555 obscure activity on these faults. The DEM (Figure 9) also shows that the many of the major river
556 systems have developed parallel to the NE-SW faults on Makira and the current mapping of the
557 structures may underestimate the faulting as a result of fluvial erosion obscuring fault traces.

Furthermore, the topographic lineament analysis undertaken here has revealed new lineaments on both islands that have previously not been recognised (Figures 2, 4 and 9), although a greater number have been identified on Makira than on Guadalcanal. On Guadalcanal, previously mapped faults are consistent with the new lineament analysis (Figure 4). These faults are described as high-angle structures with vertical slip and a minor strike-slip component of motion, which are mainly confined to the underlying basement (Coleman, 1960). Therefore, it is likely that the new lineaments mapped here for Guadalcanal are the surface expression of the NW-SE-striking vertical (normal?) slip faults. By contrast, many more potential faults have been identified on Makira through lineament analysis than are present on the DoS (1969) map (Figure 9). These lineaments show a dominant NE-SW trend, previously determined as the 'master' faults set by Petterson et al. (2009) and are consistent with their partial mapping of the eastern part of the island. Petterson et al. (2009) state that these faults are also normal faults similar to those on Guadalcanal. The normal faults are indicative of upper plate extension, which has been described in subduction zones worldwide particularly where plate motion is oblique to the trench (e.g., Whittaker et al., 1992; Upton et al., 2003). While the normal faults described here are not responsible for the > 7.0 M_w megathrust earthquakes, active normal faults > 12 km in length could still generate earthquakes of 5.0 - 6.0 M_w (Wells and Coppersmith, 1994).

Secondly, there is a weak relationship on Makira between uplift and various landscape metrics, including relief and channel steepness. While k_{sn} values are not directly convertible into rock uplift rates, river profile analysis can be used to identify steeper channels and thus regions more likely to be experiencing relatively higher erosion and uplift rates. There is a well-documented linkage between landscape transience, river incision and landsliding especially where bedrock lithologies are similar (Ouimet et al., 2007; Gallen et al., 2011; Bennett et al., 2016). As the knickpoint migrates through the system, the downstream portion of the river steepens and incises to the new base-level. Consequently, gorge formation and development of hillslopes with angles > 45° are typical. Landslides have been shown to be common downstream of knickpoints and are a key process in the erosion of landscapes (e.g., Gallen et al., 2011; Bennett et al., 2016). Therefore, in river reaches downstream of the knickpoints on Guadalcanal and Makira, the incidence of landslides will likely be higher than upstream of the knickpoints.

In addition to landslides triggered by incision, earthquakes induce many landslides (Keefer, 1984); where the density of landsliding increases with earthquake magnitude (Keefer, 2000; Meunier et al.,

2008). Furthermore, earthquakes likely 'prime' landscapes increasing the likelihood of further landsliding; a concept referred to as preconditioning (Parker et al., 2015). Therefore, in the Solomon Islands landslides may be triggered co-seismically or by rainfall but present a clear hazard along steep catchments.

6 Conclusions

Topographic lineament and river profile analyses, using DEMs, were undertaken on the islands of Guadalcanal and Makira that form the southernmost part of the Solomon Island chain and have well defined uplift fields. Situated on two different arc segments the bedrock geology and fluvial geomorphology shows marked similarities and differences between the two islands. Lineament analysis is consistent with existing mapping, showing that both islands have previously unrecognised NE-SW and ESE-WNW striking faults, likely to be extensional in nature. Fifty-seven rivers for Guadalcanal and forty-one rivers for Makira were selected for river profile analysis. On both islands, rivers flowing to the north were overall less steep and longer than the rivers flowing to the south coast and northern rivers were more likely to contain slope-break knickpoints. There is a weak correlation between knickpoint elevation and topographic relief for both Makira and Guadalcanal, but for Makira there is no clear correlation between relief and k_{sn}, while the rivers of Guadalcanal do have a weak correlation between these parameters. By contrast, there is a weak positive linear relationship between river steepness index and interpolated uplift rates for Makira, as predicted by stream-power erosion laws, which allows K, the erosion coefficient, to be calculated. The origin of these knickpoints is likely to be the result of tectonic uplift along the arc, and reinforces that these islands are subject to not only high-magnitude earthquakes, but that river incision and knickpoint migration are also likely to result in hillslope instabilities and landsliding. The differences between the geomorphic response of the two islands, given climatic similarities, is probably the result of the more complex bedrock geology of Guadalcanal in comparison to Makira, highlighting the importance not only of tectonic but lithological control on landscape evolution. The differences in the bedrock geology, structural grain and geomorphology also support the hypothesis that these islands are located on different segments of the Solomon Arc.

7 Conflict of Interest

The author declares that the research was conducted in the absence of any commercial or financial relationships that could be construed as a potential conflict of interest.

8 Funding

No external funding supported this research.

9 Acknowledgments

Thanks to the guest editor - Afroz Shah, two anonymous reviewers, Jesse Zondervan and Alex Whittaker for useful discussions and comments that have improved this research.

10 References

Abram N.J., McGregor H. V., Gagan M.K., Hantoro W.S., Suwargadi B.W. 2009. Oscillations in the southern extent of the Indo-Pacific Warm Pool during the mid-Holocene. Quaternary Science Reviews 28: 2794–2803.

Balco, G., Stone, J.O, Lifton, N.A, and Dunai, T.J. 2008. A complete and easily accessible means of calculating surface exposure ages or erosion rates from ^{10}Be and ^{26}Al measurements. Quaternary Geochronology, 3: 174-195

van der Beek, P., Champel, B. and Mugnier, JL., 2002. Control of detachment dip on drainage development in regions of active fault-propagation folding, Geology, 30(5), 471–474.

Bennett G.L., Miller S.R., Roering J.J., Schmidt D.A. 2016. Landslides, threshold slopes, and the survival of relict terrain in the wake of the Mendocino Triple Junction. Geology 44 : 363–366.

Bernard T., Sinclair H. D., Gailleton B., Mudd S. M., Ford M. 2019. Lithological control on the post-orogenic topography and erosion history of the Pyrenees. Earth and Planetary Science Letters, 518, 53–66. https://doi.org/10.1016/J.EPSL.2019.04.034

Bishop P., Hoey T.B., Jansen J.D., Lexartza Artza I. 2005. Knickpoint recession rate and catchment area: The case of uplifted rivers in Eastern Scotland. Earth Surface Processes and Landforms 30FT:

767–778.

Brocard, G. Y., & Van der Beek, P. A. (2006). Influence of incision rate, rock strength, and bedload supply on bedrock river gradients and valley-flat widths: Field-based evidence and calibrations from western Alpine rivers (southeast France). Geological Society of America Special Papers, 398, 101-126.

Boulton S.J., Stokes M. 2018. Which DEM is best for analyzing fluvial landscape development in mountainous terrains? Geomorphology 310: 168-187.

Boulton S.J., Stokes M., Mather A.E. 2014. Transient fluvial incision as an indicator of active faulting and Plio-Quaternary uplift of the Moroccan High Atlas. Tectonophysics, 633: 16-33.

Boulton S.J., Whittaker A.C. 2009. Quantifying the slip rates, spatial distribution and evolution of active normal faults from geomorphic analysis: Field examples from an oblique-extensional graben, southern Turkey. Geomorphology 104: 299–316.

Burbank, D. W., & Anderson, R. S. 2011. Tectonic Geomorphology: Second Edition. Tectonic Geomorphology: Second Edition. https://doi.org/10.1002/9781444345063

Castillo M., Ferrari L., Muñoz-Salinas E. 2017. Knickpoint retreat and landscape evolution of the Amatlán de Cañas half-graben (northern sector of Jalisco Block, western Mexico). Journal of South American Earth Sciences 77 : 108–122.

Chen M-C., Frohlich C., Taylor F.W., Burr G., van Ufford A.Q. 2011. Arc segmentation and seismicity in the Solomon Islands arc, SW Pacific. Tectonophysics 507 : 47–69. 10.1016/J.TECTO.2011.05.008

Cowley S., Mann P., Coffin M.F., Shipley T.H. 2004. Oligocene to Recent tectonic history of the Central Solomon intra-arc basin as determined from marine seismic reflection data and compilation of onland geology. Tectonophysics 389 : 267–307. DOI: 10.1016/J.TECTO.2004.01.008

Crosby BT, Whipple K.X. 2006. Knickpoint initiation and distribution within fluvial networks: 236 waterfalls in the Waipaoa River, North Island, New Zealand. Geomorphology 82 : 16–38. DOI: 10.1016/j.geomorph.2005.08.023

Cyr AJ, Granger DE, Olivetti V, Molin P. 2014. Distinguishing between tectonic and lithologic

controls on bedrock channel longitudinal profiles using cosmogenic 10Be erosion rates and channel steepness index. Geomorphology 209 : 27–38. DOI: 10.1016/j.geomorph.2013.12.010

D'Arcy, M. and Whittaker, A.C., 2014. Geomorphic constraints on landscape sensitivity to climate in tectonically active areas. Geomorphology, 204, pp.366-381.

D.o.S. 1969. Geological Map of the Solomon Islands . 2nd Editio. Department of Geological Surveys

DiBiase RA, Whipple KX, Heimsath AM, Ouimet WB. 2010. Landscape form and millennial erosion rates in the San Gabriel Mountains, CA. Earth and Planetary Science Letters 289 : 134–144. DOI: 10.1016/J.EPSL.2009.10.036

Farr, T.G., Rosen, P.A., Caro, E., Crippen, R., Duren, R., Hensley, S., Kobrick, M., Paller, M., Rodriguez, E., Roth, L., Seal, D., Shaffer, S., Shimada, J., Umland, J., Werner, M., Oskin., M., Burbank, D., Alsdorf, D., 2007. The shuttle radar topography mission. Reviews of geophysics, 45(2).

Ferrier KL, Huppert KL, Perron JT. 2013. Climatic control of bedrock river incision. Nature 496 : 206–9. DOI: 10.1038/nature11982

Finnegan, N. J., Roe, G., Montgomery, D. R., & Hallet, B. (2005). Controls on the channel width of rivers: Implications for modeling fluvial incision of bedrock. Geology, 33(3), 229–232. https://doi.org/10.1130/G21171.1

Forte, A.M., Yanites, B.J. and Whipple, K.X., (2016). Complexities of landscape evolution during incision through layered stratigraphy with contrasts in rock strength. Earth Surface Processes and Landforms, 41(12), 1736-1757

Gallen SF, Wegmann KW. 2017. River profile response to normal fault growth and linkage: an example from the Hellenic forearc of south-central Crete, Greece. Earth Surf. Dynam. 5 : 161–186. DOI: 10.5194/esurf-5-161-2017

Gallen SF, Wegmann KW, Frankel KL, Hughes S, Lewis RQ, Lyons N, Paris P, Ross K, Bauer JB, Witt AC. 2011. Hillslope response to knickpoint migration in the Southern Appalachians: implications for the evolution of post-orogenic landscapes. Earth Surface Processes and Landforms 36 : 1254–1267. DOI: 10.1002/esp.2150

697 Ganas, A., Pavlides, S. and Karastathis, V., 2005. DEM-based morphometry of range-front
698 escarpments in Attica, central Greece, and its relation to fault slip rates. *Geomorphology*, *65*(3-4),
699 301-319.

700 Goldrick G, Bishop P. 2007. Regional analysis of bedrock stream long profiles: evaluation of Hack's
701 SL form, and formulation and assessment of an alternative (the DS form). Earth Surface Processes
702 and Landforms 32 : 649–671. DOI: 10.1002/esp.1413

703 Gosse, J. C. and Phillips, F. M. (2001) 'Terrestrial in situ cosmogenic nuclides: theory and
704 application', *Quaternary Science Reviews*, 20(14), pp. 1475–1560. doi: 10.1016/S0277-
705 3791(00)00171-2.

706 Hackman BD. 1980. The Geology of Guadalcanal, Solomon Islands . HM Stationary Office

707 Harel, M. A., Mudd, S. M. and Attal, M. (2016) 'Global analysis of the stream power law parameters
708 based on worldwide 10Be denudation rates', *Geomorphology*. doi: 10.1016/j.geomorph.2016.05.035.

709 Harkins N, Kirby E, Heimsath A, Robinson R, Reiser U. 2007. Transient fluvial incision in the
710 headwaters of the Yellow River, northeastern Tibet, China. Journal of Geophysical Research: Earth
711 Surface 112 : 1–21. DOI: 10.1029/2006JF000570

712 Haviv I, Enzel Y, Whipple KX, Zilberman E, Matmon A, Stone J, Fifield KL. 2010. Evolution of
713 vertical knickpoints (waterfalls) with resistant caprock: Insights from numerical modeling. Journal of
714 Geophysical Research: Earth Surface 115 DOI: 10.1029/2008JF001187

715 Johnson CB, Furlong KP, Kirby E. 2009. Integrated geomorphic and geodynamic modeling of a
716 potential blind thrust in the San Francisco Bay area, California. Tectonophysics 471 : 319–328. DOI:
717 10.1016/j.tecto.2009.03.002

718 Katz, O., Reches, Z., Roegiers, J.-C., 2000. Evaluation of mechanical rock properties using a
719 Schmidt Hammer. International Journal of rock mechanics and mining sciences 37, 723-728.

720 Keefer D.K. 1984. Landslides caused by earthquakes. Bulletin of the Geological Society America, 95
721 406-421.

722 Keefer D.K., 2000. Statistical analysis of an earthquake-induced landslide distribution—the 1989
723 Loma Prieta, California event. Engineering Geology, 58 213-249

724 Kent E, Boulton SJ, Whittaker AC, Stewart IS, Cihat Alçiçek M. 2017. Normal fault growth and
725 linkage in the Gediz (Alaşehir) Graben, Western Turkey, revealed by transient river long-profiles and
726 slope-break knickpoints. Earth Surface Processes and Landforms 42 DOI: 10.1002/esp.4049

727 Kirby E, Whipple K. 2001. Quantifying differential rock-uplift rates via stream profile analysis.
728 Geology 29 : 415. DOI: 10.1130/0091-7613(2001)029<0415:QDRURV>2.0.CO;2

729 Kirby E, Whipple KX. 2012. Expression of active tectonics in erosional landscapes. Journal of
730 Structural Geology 44 : 54–75. DOI: 10.1016/j.jsg.2012.07.009

731 Kirby, E., Whipple, K. X., Tang, W., & Chen, Z. (2003). Distribution of active rock uplift along the
732 eastern margin of the Tibetan Plateau: Inferences from bedrock channel longitudinal profiles. Journal
733 of Geophysical Research: Solid Earth, 108(B4). https://doi.org/10.1029/2001jb000861

734 Kuo Y-T, Ku C-S, Chen Y-G, Wang Y, Lin Y-NN, Chuang RY, Hsu Y-J, Taylor FW, Huang B-S,
735 Tung H. 2016. Characteristics on fault coupling along the Solomon megathrust based on GPS
736 observations from 2011 to 2014. Geophysical Research Letters 43 : 8519–8526. DOI:
737 10.1002/2016GL070188

738 Lambeck K, Chappell J. 2001. Sea Level Change Through the Last Glacial Cycle. Science 292 : 679
739 LP – 686. DOI: 10.1126/science.1059549

740 Liu, Z., Han, L., Boulton, S.J., Wu, T. and Guo, J., 2019. Quantifying the transient landscape
741 response to active faulting using fluvial geomorphic analysis in the Qianhe Graben on the southwest
742 margin of Ordos, China. Geomorphology, https://doi.org/10.1016/j.geomorph.2019.106974

743 Mann P, Taylor FW, Lagoe MB, Quarles A, Burr G. 1998. Accelerating late Quaternary uplift of the
744 New Georgia Island Group (Solomon island arc) in response to subduction of the recently active
745 Woodlark spreading center and Coleman seamount. Tectonophysics 295 : 259–306. DOI:
746 10.1016/S0040-1951(98)00129-2

747 Malamud, B. D. *et al.* (2004) 'Landslide inventories and their statistical properties', *Earth Surface*
748 *Processes and Landforms*, 29(6), pp. 687–711. doi: 10.1002/esp.1064.

749 Marliyani GI, Arrowsmith JR, Whipple KX. 2016. Characterization of slow slip rate faults in humid
750 areas: Cimandiri fault zone, Indonesia. Journal of Geophysical Research: Earth Surface 121 : 2287–

2308. DOI: 10.1002/2016JF003846

Menier, D., Mathew, M., Pubellier, M., Sapin, F., Delcaillau, B., Siddiqui, N., Ramkumar, M. and Santosh, M., 2017. Landscape response to progressive tectonic and climatic forcing in NW Borneo: Implications for geological and geomorphic controls on flood hazard. Scientific reports, 7(1), p.457.

Menking JA, Han J, Gasparini NM, Johnson JPL. 2013. The effects of precipitation gradients on river profile evolution on the Big Island of Hawai'i. GSA Bulletin 125 : 594–608. DOI: 10.1130/B30625.1

Meunier, P., Hovius, N. and Haines, J.A., 2008. Topographic site effects and the location of earthquake induced landslides. Earth and Planetary Science Letters, 275(3-4), 221-232.

Miller SR. 2013. Neogene rejuvenation of central Appalachian topography: Evidence for differential rock uplift from stream profiles and erosion rates. Earth and Planetary Science Letters 369–370 : 1–12. DOI: 10.1016/J.EPSL.2013.04.007

Miller SR, Baldwin SL, Fitzgerald PG. 2012. Transient fluvial incision and active surface uplift in the Woodlark Rift of eastern Papua New Guinea. Lithosphere 4 : 131–149. DOI: 10.1130/L135.1

Miura S, Suyehiro K, Shinohara M, Takahashi N, Araki E, Taira A. 2004. Seismological structure and implications of collision between the Ontong Java Plateau and Solomon Island Arc from ocean bottom seismometer–airgun data. Tectonophysics 389 : 191–220. DOI: 10.1016/j.tecto.2003.09.029

Mizera M, Little TA, Biemiller J, Ellis S, Webber S, Norton KP. 2019. Structural and Geomorphic Evidence for Rolling-Hinge Style Deformation of an Active Continental Low-Angle Normal Fault, SE Papua New Guinea. Tectonics 0 DOI: 10.1029/2018TC005167

Neely AB, Bookhagen B, Burbank DW. 2017. An automated knickzone selection algorithm (KZ-Picker) to analyze transient landscapes: Calibration and validation. Journal of Geophysical Research: Earth Surface 122 DOI: 10.1002/2017JF004250

O'Leary DW, Friedman JD, Pohn HA. 1976. Lineament, linear, lineation: Some proposed new standards for old terms. Geological Society ofAmerica Bulletin 87: 1463 –1469.

Oguchi, T., Aoki, T. and Matsuta, N., 2003. Identification of an active fault in the Japanese Alps from DEM-based hill shading. *Computers & Geosciences*, *29*(7), pp.885-891.

778 Onorati G, Poscolieri M, Ventura R, Chiarini V, Crucilla U. 1992. The digital elevation
779 model of Italy for geomorphology and structuralgeology. Catena 19: 147–178.

780 Ortega J a., Wohl E, Livers B. 2013. Waterfalls on the eastern side of Rocky Mountain National
781 Park, Colorado, USA. Geomorphology 198 : 37–44. DOI: 10.1016/j.geomorph.2013.05.010

782 Ouimet WB, Whipple KX, Granger DE. 2009. Beyond threshold hillslopes: Channel adjustment to
783 base-level fall in tectonically active mountain ranges. Geology 37 : 579–582. DOI:
784 10.1130/G30013A.1

785 Ouimet WB, Whipple KX, Royden LH, Sun Z, Chen Z. 2007. The influence of large landslides on
786 river incision in a transient landscape: Eastern margin of the Tibetan Plateau (Sichuan, China). GSA
787 Bulletin 119 : 1462–1476. DOI: 10.1130/B26136.1

788 Parker, R.N., Hancox, G.T., Petley, D.N., Massey, C.I., Densmore, A.L. and Rosser, N.J., 2015.
789 Spatial distributions of earthquake-induced landslides and hillslope preconditioning in northwest
790 South Island, New Zealand. Earth surface dynamics., 3(4), 501-525.

791 Petterson M. et al. 1999. Geological–tectonic framework of Solomon Islands, SW Pacific: crustal
792 accretion and growth within an intra-oceanic setting. Tectonophysics 301 : 35–60. DOI:
793 10.1016/S0040-1951(98)00214-5

794 Petterson MG, Neal CR, Mahoney JJ, Kroenke LW, Saunders AD, Babbs TL, Duncan RA, Tolia D,
795 McGrail B. 1997. Structure and deformation of north and central Malaita, Solomon Islands: tectonic
796 implications for the Ontong Java Plateau-Solomon arc collision, and for the fate of oceanic plateaus.
797 Tectonophysics 283 : 1–33. DOI: 10.1016/S0040-1951(97)00206-0

798 Phillips JD, Lutz JD. 2008. Profile convexities in bedrock and alluvial streams. Geomorphology 102 :
799 554–566. DOI: 10.1016/j.geomorph.2008.05.042

800 Pipaud, I., Loibl, D. and Lehmkuhl, F. (2015) 'Evaluation of TanDEM-X elevation data for
801 geomorphological mapping and interpretation in high mountain environments — A case study from
802 SE Tibet, China', *Geomorphology*, 246, pp. 232–254. doi: 10.1016/j.geomorph.2015.06.025.

803 Regalla C, Kirby E, Fisher D, Bierman P. 2013. Active forearc shortening in Tohoku, Japan:
804 Constraints on fault geometry from erosion rates and fluvial longitudinal profiles. Geomorphology

195 : 84–98. DOI: 10.1016/j.geomorph.2013.04.029

Rao, G. *et al.* (2017) 'Relationship between landslides and active normal faulting in the epicentral area of the AD 1556 M~8.5 Huaxian Earthquake, SE Weihe Graben (Central China)', *Journal of Earth Science*, 28(3), pp. 545–554. doi: 10.1007/s12583-017-0900-z.

Ridgway J. 1987. Neogene displacements in the Solomon Islands Arc. Tectonophysics 133 : 81–93. DOI: 10.1016/0040-1951(87)90282-4

Roy, S. G., Tucker, G. E., Koons, P. O., Smith, S. M., & Upton, P. (2016). A fault runs through it: Modeling the influence of rock strength and grain-size distribution in a fault-damaged landscape. Journal of Geophysical Research: Earth Surface, 121(10), 1911–1930. https://doi.org/10.1002/2015JF003662

Seidl MA, Dietrich WE, Kirchner JW. 1994. Longitudinal Profile Development into Bedrock: An Analysis of Hawaiian Channels. The Journal of Geology 102 : 457–474. DOI: 10.1086/629686

Seidl MA, Finkel RC, Caffee MW, Hudson GB, Dietrich WE. 1997. Cosmetic Isotope Analyses Applied to River Longitudinal Profile Evolution: Problems and Interpretations. Earth Surface Processes and Landforms 22 : 195–209. DOI: 10.1002/(SICI)1096-9837(199703)22:3<195::AID-ESP748>3.0.CO;2-0

Sklar, L. S. and Dietrich, W. E. (2006) 'The role of sediment in controlling steady-state bedrock channel slope: Implications of the saltation-abrasion incision model', *Geomorphology*, 82(1–2), pp. 58–83. doi: 10.1016/j.geomorph.2005.08.019.

Smith, MJ and Clark, CD, 2005. Methods for the visualization of digital elevation models for landform mapping. Earth Surface Processes and Landforms, 30(7), 885-900.

Smith MJ, Clark CD, Wise SM. 2001. Mapping glacial lineaments from satellite imagery: an assessment of the problems and development of best procedure. Slovak Geological Magazine 7: 263 –274.

Snyder NP, Whipple KX, Tucker GE, Merritts DJ. 2000. Stream profiles in the Mendocino triple junction region, northern California. GSA Bulletin 112 : 1250–1263.

Stock, J.D. and Montgomery, D.R., 1999. Geologic constraints on bedrock river incision using the

832 stream power law. Journal of Geophysical Research: Solid Earth, 104(B3), pp.4983-4993.

833 Tarboton, D. G., R. L. Bras, and I. Rodriguez–Iturbe. 1991. "On the Extraction of Channel Networks
834 from Digital Elevation Data." Hydrological Processes 5: 81–100.

835 Tejada, MLG. 2002. Basement Geochemistry and Geochronology of Central Malaita, Solomon
836 Islands, with Implications for the Origin and Evolution of the Ontong Java Plateau. Journal of
837 Petrology 43 : 449–484. DOI: 10.1093/petrology/43.3.449

838 Tejada MLG, Mahoney JJ, Duncan RA, Hawkins MP. 1996. Age and Geochemistry of Basement and
839 Alkalic Rocks of Malaita and Santa Isabel, Solomon Islands, Southern Margin of Ontong Java
840 Plateau. Journal of Petrology 37 : 361–394. DOI: 10.1093/petrology/37.2.361

841 Thirumalai K, Taylor FW, Shen C-C, Lavier LL, Frohlich C, Wallace LM, Wu C-C, Sun H, Papabatu
842 AK. 2015. Variable Holocene deformation above a shallow subduction zone extremely close to the
843 trench. Nature Communications 6 : 7607.

844 Tudhope AW, Chilcott CP, McCulloch MT, Cook ER, Chappell J, Ellam RM, Lea DW, Lough JM,
845 Shimmield GB. 2001. Variability in the El Niño-Southern Oscillation Through a Glacial-Interglacial
846 Cycle. Science 291 : 1511 LP – 1517. DOI: 10.1126/science.1057969

847 Upton, P., Koons, P.O. and Eberhart-Phillips, D., 2003. Extension and partitioning in an oblique
848 subduction zone, New Zealand: Constraints from three-dimensional numerical modeling. Tectonics,
849 22(6).

850 Whipple KX. 2001. Fluvial Landscape Response Time: How Plausible Is Steady-State Denudation?
851 American Journal of Science 301 : 313–325.

852 Whipple KX. 2004. Bedrock rivers and the geomorphology of active orogens. Annual Review of
853 Earth and Planetary Sciences 32 : 151–185. DOI: 10.1146/annurev.earth.32.101802.120356

854 Whipple KX, Tucker GE. 1999. Dynamics of the stream-power river incision model: Implications for
855 height limits of mountain ranges, landscape response timescales, and research needs. Journal of
856 Geophysical Research: Solid Earth 104 : 17661–17674. DOI: 10.1029/1999JB900120

857 Whipple, K. X. and Tucker, G. E. (2002) 'Implications of sediment-flux-dependent river incision

models for landscape evolution', *J Geophys Res Solid Earth*, 107. doi: 10.1029/2000JB000044.

Whittaker AC, Boulton SJ. 2012. Tectonic and climatic controls on knickpoint retreat rates and landscape response times. Journal of Geophysical Research: Earth Surface 117

Whittaker AC, Cowie P a., Attal M, Tucker GE, Roberts GP. 2007. Bedrock channel adjustment to tectonic forcing: Implications for predicting river incision rates. Geology 35 : 103–106. DOI: 10.1130/G23106A.1

Whittaker, A., M. H. P. Bott, and G. D. 1992Waghorn, Stresses and plate boundary forces associated with subduction plate margins, Journal of Geophysical Research, 97, 11,933–11,944.

Wobus C, Whipple KX, Kirby E, Snyder N, Johnson J, Spyropolou K, Crosby B, Sheehan D. 2006. Tectonics from topography: Procedures, promise, and pitfalls. In Tectonics, Climate, and Landscape Evolution , Willett SD, Hovius N, Brandon MT, and Fisher DM (eds). Geological Society of America; 0.

Wobus CW, Hodges K V, Whipple KX. 2003. Has focused denudation sustained active thrusting at the Himalayan topographic front? Geology 31 : 861–864. DOI: 10.1130/G19730.1

Woodroffe SA, Horton BP. 2005. Holocene sea-level changes in the Indo-Pacific. Journal of Asian Earth Sciences 25 : 29–43. DOI: 10.1016/J.JSEAES.2004.01.009

Yanites, B. J., Becker, J. K., Madritsch, H., Schnellmann, M., & Ehlers, T. A. (2017). Lithologic effects on landscape response to base level changes: a modeling study in the context of the Eastern Jura Mountains, Switzerland. Journal of Geophysical Research: Earth Surface, 122(11), 2196-2222.

Ye F-Y, Barriot J-P, Carretier S. 2013. Initiation and recession of the fluvial knickpoints of the Island of Tahiti (French Polynesia). Geomorphology 186 : 162–173. DOI: 10.1016/J.GEOMORPH.2012.12.031

Data Availability Statement

The SRTM 30 m datasets used in this study can be downloaded from the USGS EarthExplorer website https://earthexplorer.usgs.gov/. The bathymetry data is an extract from the General Bathymetric chart of the Oceans (GEBCO) downloaded from https://www.gebco.net/.

Figure Captions

Figure 1. Plate tectonic setting of the Solomon Island Arc with the islands of Guadalcanal and Makira forming the southernmost major islands with Mw > 6 earthquakes for the period 1980 to present shown (USGS, 2019). Bathymetric data is the GEBCO_2019 Grid (GEBCO Compilation Group 2019). Plate velocities from Chen et al. (2011).

Figure 2. Geological maps (simplified from D.o.S, 1969) of A. Guadalcanal and B. Makira showing mapped faults and uplifted coral reef locations used to interpolate the uplift field (Chen et al., 2011).

Figure 3. Conceptual diagram showing the river long profile and slope-area graphs for rivers in steady state (A and B), rivers with a vertical step knickpoint (C and D) and rivers with a slope-break knickpoint (E and F) (adapted from Wobus et al., 2006, Kirby and Whipple, 2012). Note that the steepeness index (the intercept - k_s) increases downstream across a slope-break knickpoint but not across a vertical step knickpoint. G and H show an example of a river profile and slope-area plot, respectively, from the study area. Note: this is river 21 from the island of Makira, the green line is the raw DEM river profile and the purple is the smoothed profile.

Figure 4A. ALOS World 3D 30 m DEM (©JAXA) of Guadalcanal showing existing faults from the published mapping data (D.o.S, 1969) and inferred topographic lineaments, rose diagrams showing the orientations of both datasets are shown in the top right corner. B and C) Raw and interpreted DEM for the area shown in the blue box on part A.

Figure 5. Hillshade map derived from the 30 m SRTM DEM (USGS, 2019) for the island of Guadalcanal showing the rivers extracted for analysis shaded by k_{sn}, identified slope-break knickpoints (black circles), major faults identified from analysis of the DEM and based upon existing mapping data (D.o.S, 1969) and the interpolated uplifted field.

912

913 Figure 6. Graphs showing a range of knickpoint variables for Guadalcanal where black circles are
914 knickpoints on north flowing rivers and grey are on south flowing rivers, similarly regression lines
915 are black and grey for north and south rivers, respectively and the blue lines are for all data points. A)
916 Distance from mouth against total catchment area, B) Distance from divide against catchment area
917 above the knickpoint, C) Knickpoint elevation (above sea-level) against total catchment area and D)
918 distance from mouth against knickpoint elevation.

919

920 Figure 7. Graph showing the distance along the strike of the island axis from NW – SE against mean
921 (blue) and maximum (grey) elevation, knickpoint elevation (blue north/ orange south) and
922 interpolated uplift field for the island of Guadalcanal. Note that the maximum elevation value are
923 affected by errors in the DEM.

924

925 Figure 8) K_{sn} against distance along strike of Guadalcanal showing the difference in value for the
926 river above and below the knickpoints (where present) and k_{sn} for the whole river (where knickpoints
927 are absent). B) K_{sn} ratio (below knickpoint/above knickpoint) of rivers with knickpoints along the
928 island of Guadalcanal. C) Knickpoint elevation and D) K_{sn} against topographic relief for
929 Guadalcanal.

930

931 Figure 9A. ALOS World 3D 30 m DEM (©JAXA) of Makira showing existing faults from the
932 published mapping data (D.o.S, 1969) and inferred topographic lineaments, rose diagrams showing
933 the orientations of both datasets are shown in the top right corner. B and C) Raw and interpreted
934 DEM for the area shown in the blue box on part A.

935

936 Figure 10. Hillshade map derived from the 30 m SRTM DEM (USGS, 2019) for the island of Makira
937 showing the rivers extracted for analysis shaded by k_{sn}, identified slope-break knickpoints (black
938 circles) and major faults identified from analysis of the DEM and based upon existing mapping data
939 (D.o.S, 1969).

940

941 Figure 11. Graphs showing a range of knickpoint variables for Makira where black circles are
942 knickpoints on north flowing rivers and grey are on south flowing rivers. A) Distance from mouth
943 against total catchment area, B) Distance from divide against catchment area above the knickpoint,

C) Knickpoint elevation (above sea-level) against total catchment area and D) distance from mouth against knickpoint elevation.

Figure 12. Graph showing the distance along the strike of the island axis from NW – SE against mean (blue) and maximum (grey) elevation, knickpoint elevation (blue north/ orange south) and interpolated uplift field for the island of Makira. Note that the maximum elevation values are affected by errors in the DEM.

Figure 13. A) K_{sn} against distance along strike of Makira showing the difference in values for rivers above and below the knickpoints (where present) and k_{sn} for the whole river (where knickpoints are absent). B) K_{sn} ratio (below knickpoint/above knickpoint) of rivers along the island of Makira. Figure 8. C) Knickpoint elevation and D) K_{sn} against topographic relief for Makira.

Figure 14. A) and B) plots of k_{sn} against interpolated uplift rates of the islands of Guadalcanal and Makira, respectively.

959

960 **Tables**

									Below knickpoint			Above knickpoint			
River No	Distance along strike	Length (km)	Catchment area (km^2)	Topographic Relief (m)	KP1 elevation (m)	CA Above KP (km^2)	DFM (km)	DFD (km)	K_{sn}	θ	±	K_{sn}	θ	±	K_{sn} ratio
Guadacanal (rivers with knickpoints)															
1	14.2	11.6	25.4	60.0	443	0.40	10.5	1.0	49.8	0.7	0.3	115.1	1.0	0.4	0.4
2	14.6	13.5	29.1	72.6	526	0.88	12.2	1.2	79.2	0.7	0.2	50.1	0.4	0.2	1.6
4	24.8	13.0	81.6	49.9	612	0.24	12.2	0.8	51.3	0.8	0.2	40.0	0.6	0.3	1.3
5	24.7	26.6	81.6	49.9	476	2.35	23.1	3.5	52.6	0.6	0.2	14.0	0.3	0.3	3.7
7	30.7	28.4	70.0	55.3	243	24.44	17.8	10.6	70.9	1.8	2.1	44.5	0.4	0.2	1.6
8	34.6	19.2	45.8	51.0	355	4.73	15.8	3.4	44.6	2.0	0.6	80.7	0.7	0.3	0.6
9	36.4	12.5	18.7	45.6	341	7.81	5.0	7.5	159.8	0.5	1.4	33.9	0.5	0.2	4.7
11	52.3	68.4	396.1	56.7	391	35.78	52.8	15.6	54.3	0.6	0.4	22.9	0.2	0.3	2.4
12	56	33.1	147.3	37.6	531	13.03	28.5	4.6	116.7	0.8	1.1	42.0	0.8	0.4	2.8
13	59	70.0	650.8	63.5	1519	3.08	67.1	2.9	117.9	0.8	0.1	47.6	0.9	0.5	2.5
17	99.4	25.2	94.1	44.3	269	15.59	16.3	8.9	175.8	5.9	3.4	110.0	0.5	0.1	1.6
18	104.4	36.0	104.1	65.0	406	34.64	22.5	13.5	102.7	2.5	1.8	74.9	0.6	0.1	1.4
20	115.1	30.5	62.1	80.5	1318	0.36	29.6	1.0	118.5	1.1	0.2	69.9	1.2	0.2	1.7
					825	2.63	27.0	3.6				82.8	1.1	0.3	
22	122	20.8	169.9	81.8	543	2.72	18.7	2.1	89.6	0.9	0.6	30.8	0.6	0.2	2.9

26	136.7	9.4	29.4	69.7	466	1.07	7.9	1.5	80.3	0.7	0.3	58.1	0.4	0.1	1.4
27	140.1	8.3	13.3	84.7	265	4.80	5.2	3.1	164.0	6.0	3.8	90.5	0.5	0.1	1.8
29	137.4	12.4	23.3	106.9	541	4.52	9.4	3.0	180.7	0.5	1.4	145.1	0.5	0.1	1.2
33	116.5	11.4	20.8	125.6	847	0.38	10.6	0.8	119.9	0.8	0.2	74.7	0.3	0.2	1.6
34	107.3	15.1	29.8	113.3	826	5.99	11.6	3.4	192.2	2.3	0.5	81.3	0.5	0.1	2.4
38	87.2	12.0	33.1	110.2	678	4.06	8.6	3.3	132.5	1.4	0.7	48.1	0.4	0.1	2.8
44	46.8	33.3	339.0	79.9	1055	7.94	28.5	4.8	252.0	2.7	0.7	101.2	0.6	0.1	2.5
50	7.8	15.0	42.0	55.3	322	6.21	10.3	4.7	60.4	2.5	0.9	34.6	0.5	0.3	1.7
52	1.8	16.3	35.7	52.4	402	2.87	11.8	4.5	72.5	1.2	0.9	33.2	0.7	0.2	2.2
53	2	13.4	15.2	50.6	334	4.78	9.1	4.4	52.3	0.4	1.6	48.1	0.5	0.1	1.1

Guadacanal (rivers without knickpoints)

3	19.5	12.0	21.1	36.8	47.0	0.6	0.2
6	27.8	22.5	45.9	45.4	33.6	0.4	0.1
10	43.2	20.0	57.7	46.2	42.3	0.4	0.1
14	72.8	22.0	244.9	85.9	53.1	0.6	0.1
15	86	47.5	346.3	56.0	59.6	0.8	0.3
16	96	22.0	199.6	62.5	65.6	0.5	0.2
19	112.9	40.0	109.5	67.0	70.5	0.5	0.1
21	121.4	35.0	105.5	84.1	83.1	0.4	0.1
23	125.1	10.0	15.7	66.8	65.9	0.6	0.3

24	128.7	22.0	69.8	80.1	60.2	0.6	0.1
25	132.2	21.0	41.8	52.8	70.5	0.4	0.1
28	137.5	9.0	13.6	90.0	112.8	0.7	0.1
30	133.9	33.0	46.4	103.6	126.3	0.9	0.1
31	121.7	15.0	33.3	101.3	113.9	0.5	0.1
32	117.9	20.0	48.5	117.6	128.9	0.5	0.1
35	103.7	15.0	71.3	107.0	168.9	0.4	0.1
36	96.5	12.0	44.2	109.2	70.1	0.5	0.1
37	88.8	11.5	27.8	111.0	58.9	0.4	0.1
39	83.5	8.5	21.8	71.5	92.9	0.2	0.1
40	79.4	14.0	47.2	131.1	145.5	0.3	0.1
41	73	9.5	18.1	140.6	181.4	0.1	0.1
42	70.8	18.0	54.2	104.6	193.1	0.2	0.1
43	62.6	16.0	30.7	142.4	185.6	0.4	0.1
45	40.1	14.0	30.0	67.0	68.0	0.4	0.2
46	36.5	17.0	55.6	68.7	83.4	0.9	0.2
47	28.4	8.0	26.6	67.6	81.7	0.7	0.1
48	21.1	21.0	105.1	64.5	82.4	0.5	0.2

49	15.8	20.5	80.2	57.0					64.8	0.3	0.2				
51	3.9	19.5	78.4	50.2					40.5	0.4	0.2				
Makira (rivers with knickpoints)															
1	4.7	16.6	46.3	293.0	163.0	10.22	11.3	5.3	46.4	-0.5	3.0	17.2	2.4	15.8	0.4
2	16.7	9.7	27.0	258.0	377.0	0.12	9.0	0.3	40.9	1.1	0.3	20.0	0.2	1.1	0.5
5	27.0	11.3	15.4	154.0	161.0	7.47	5.9	5.4	60.0	0.3	3.5	48.2	1.3	3.4	0.8
					252.0	3.22	8.0	3.3				9.8	0.6	0.3	4.9
6	33.0	8.0	13.6	270.0	216.0	2.73	4.6	3.3	55.5	2.4	1.9	26.6	0.8	0.4	0.5
12	53.3	17.3	63.5	189.0	336.0	0.54	16.4	0.9	34.9	1.3	0.3	45.8	1.5	0.4	1.3
13	55.3	29.2	226.2	269.0	193.0	0.15	28.6	0.6	25.2	0.8	0.2	6.1	0.4	1.8	0.2
14	59.6	14.8	54.0	337.0	244.0	2.56	12.5	2.4	33.2	1.0	0.5	24.9	0.5	0.3	0.7
17	69.9	30.3	82.5	312.0	722.0	1.54	28.3	2.1	63.4	0.1	0.4	6.8	0.9	0.3	0.1
19	88.2	35.8	237.3	326.0	722.0	58.65	21.5	14.3	69.5	1.7	3.8	22.6	0.3	0.2	0.3
20	96.0	7.9	9.5	155.0	298.0	5.43	3.6	4.3	132.4	2.6	1.3	53.4	0.0	0.4	2.5
23	115.8	13.1	21.1	237.0	390.0	1.42	11.1	1.9	49.3	1.0	0.3	31.3	1.4	0.9	1.6
					512.0	0.17	12.3	0.7				20.8	0.4	0.4	1.5
24	117.5	32.7	158.7	266.0	485.0	5.24	29.6	3.1	46.6	0.9	0.3	55.5	0.6	0.2	0.8
25	117.9	11.8	21.0	137.0	193.0	1.18	10.2	1.7	31.0	0.7	0.7	32.0	0.5	0.3	1.0
26	126.0	1	15.4	156.0	184.0	1.16	8.3	1.7	22.1	1.7	0.8	41.8	0.7	0.2	0.5
30	96.9	6.8	10.9	240.0	518.0	0.15	6.4	0.6	104.4	0.8	0.1	29.9	0.2	0.4	3.5
36	70.9	18.0	30.4	235.0	807.0	1.15	35.0	1.4	59.4	0.8	0.1	30.5	0.9	0.4	1.9
38	51.0	8.9	20.0	269.0	260.0	0.39	7.9	1.0	33.5	0.9	0.4	26.4	1.2	0.3	1.3

40	28.9	6.1	18.6	257.0	163.0	2.76	4.0	2.0	49.7	0.8	2.3	29.7	0.8	0.1	1.7
41	18.0	8.0	22.6	148.0	190.0	0.08	7.5	0.5	27.2	0.6	0.2	14.3	0.7	0.5	1.9
Makira (rivers without knickpoints)															
3	21.6	15.0	37.8	299.0	3				38.0	0.5	0.1				
4	25.0	12.0	22.0	361.0	4				58.7						
7	34.2	14.0	22.7	164.0	7				9.5	0.7	0.2				
8	36.3	19.0	50.6	238.0	8				15.1	1.0	0.4				
9	37.1	25.0	80.4	165.0	9				17.8	0.7	0.1				
10	44.0	26.0	18.4	191.0	10				11.0	0.6	0.3				
11	45.7	14.0	88.7	182.0	11				48.1	0.5	0.1				
15	67.1	27.0	94.7	310.0	15				45.6	0.4	0.1				
16	68.4	38.0	118.7	362.0	16				23.2	0.4	0.2				
18	82.5	31.0	246.6	315.0	18				29.7	0.1	0.3				
21	102.0	26.0	16.8	274.0	21				67.4	0.3	0.1				
22	108.0	25.0	108.9	236.0	22				64.2	0.4	0.1				
27	118.0	9.5	65.9	288.0	27				34.3	0.6	0.1				
28	106.0	8.2	33.7	194.0	28				109.4	0.7	0.2				
29	100.0	5.1	10.2	355.0	29				97.3	0.3	0.2				
31	94.5	11.2	29.5	335.0	31				71.9	0.5	0.1				
32	91.2	8.3	11.3	288.0	32				65.3	0.4	0.1				
33	89.5	8.9	28.3	266.0	33				48.4	1.2	0.3				
34	76.3	14.8	44.4	248.0	34				45.7	0.8	0.1				
35	75.5	8.0	17.0	284.0	35				95.5	0.6	0.1				
37	48.7	9.8	36.5	246.0	37				24.7	0.6	0.2				

39	30.7	6.5	12.3	137.0	39		10.0	0.7	0.2

961

Figure 1.TIF

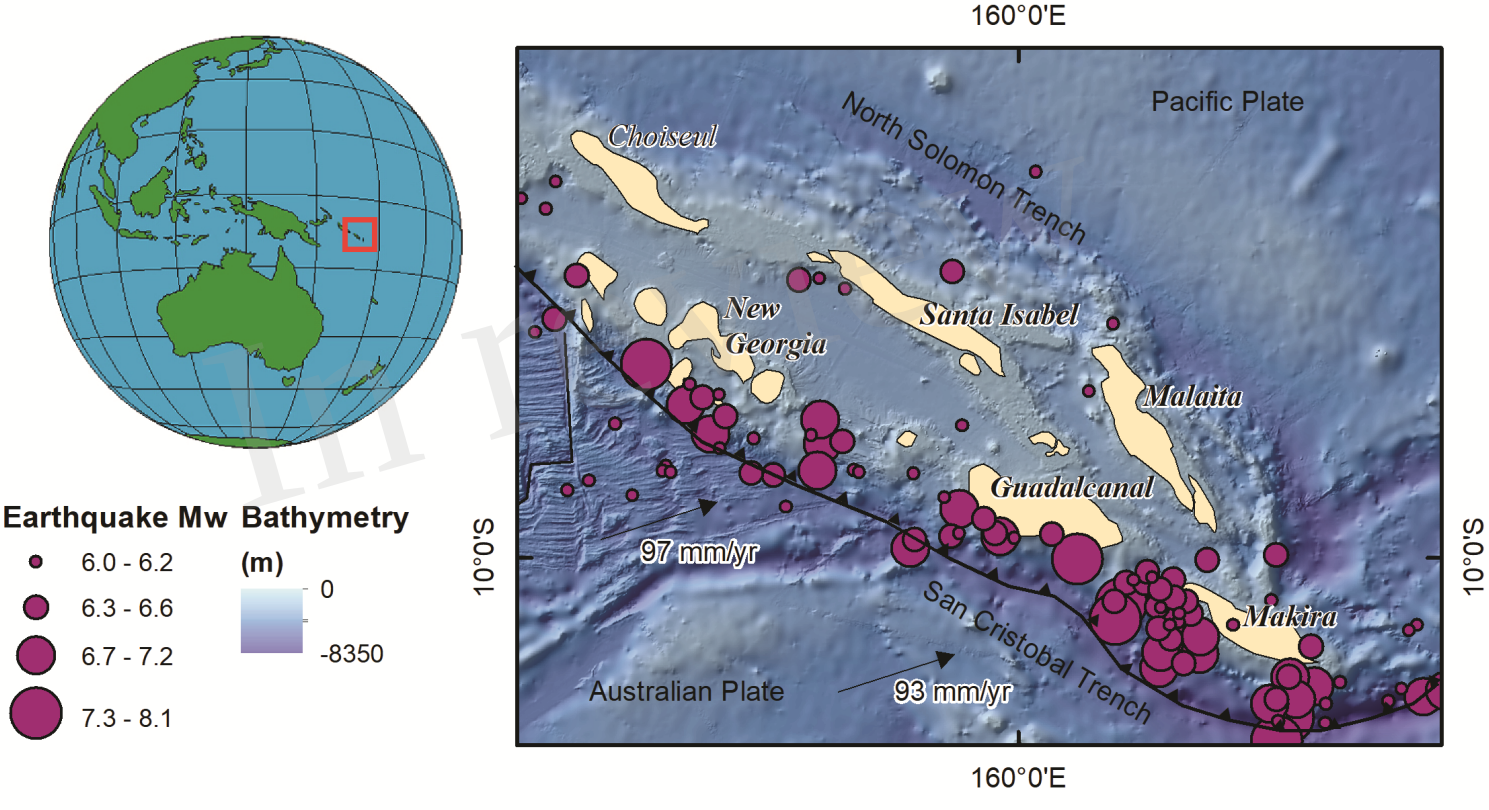
160°0'E
Pacific Plate
Choiseul
North Solomon Trench
New Georgia
Santa Isabel
Malaita
Guadalcanal
Makira
San Cristobal Trench
97 mm/yr
93 mm/yr
Australian Plate
10°0'S
10°0'S
160°0'E
Earthquake Mw
6.0 - 6.2
6.3 - 6.6
6.7 - 7.2
7.3 - 8.1
Bathymetry
(m)
0
-8350

Figure 2.TIF

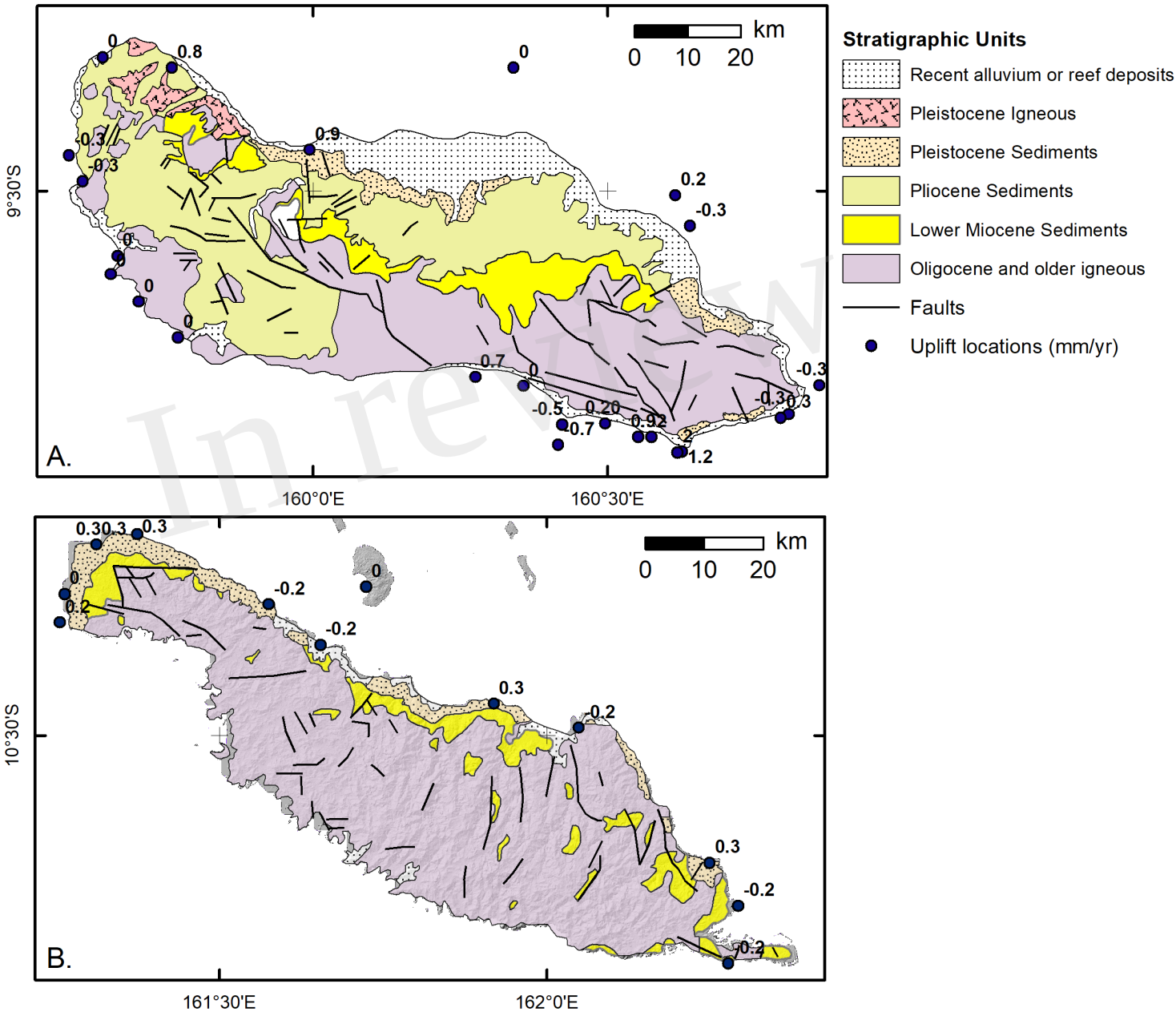

Figure 3.TIF

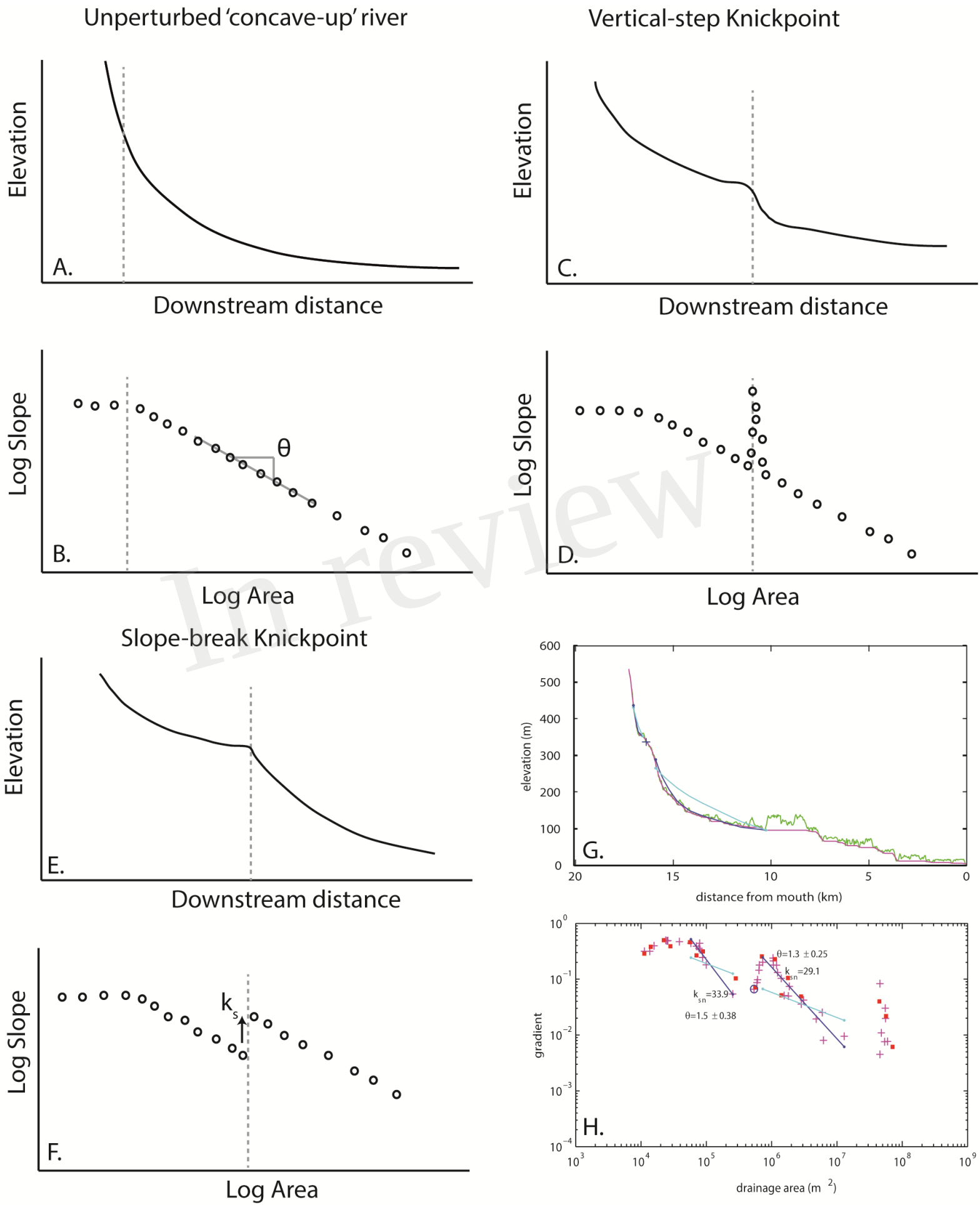

Figure 4.TIF

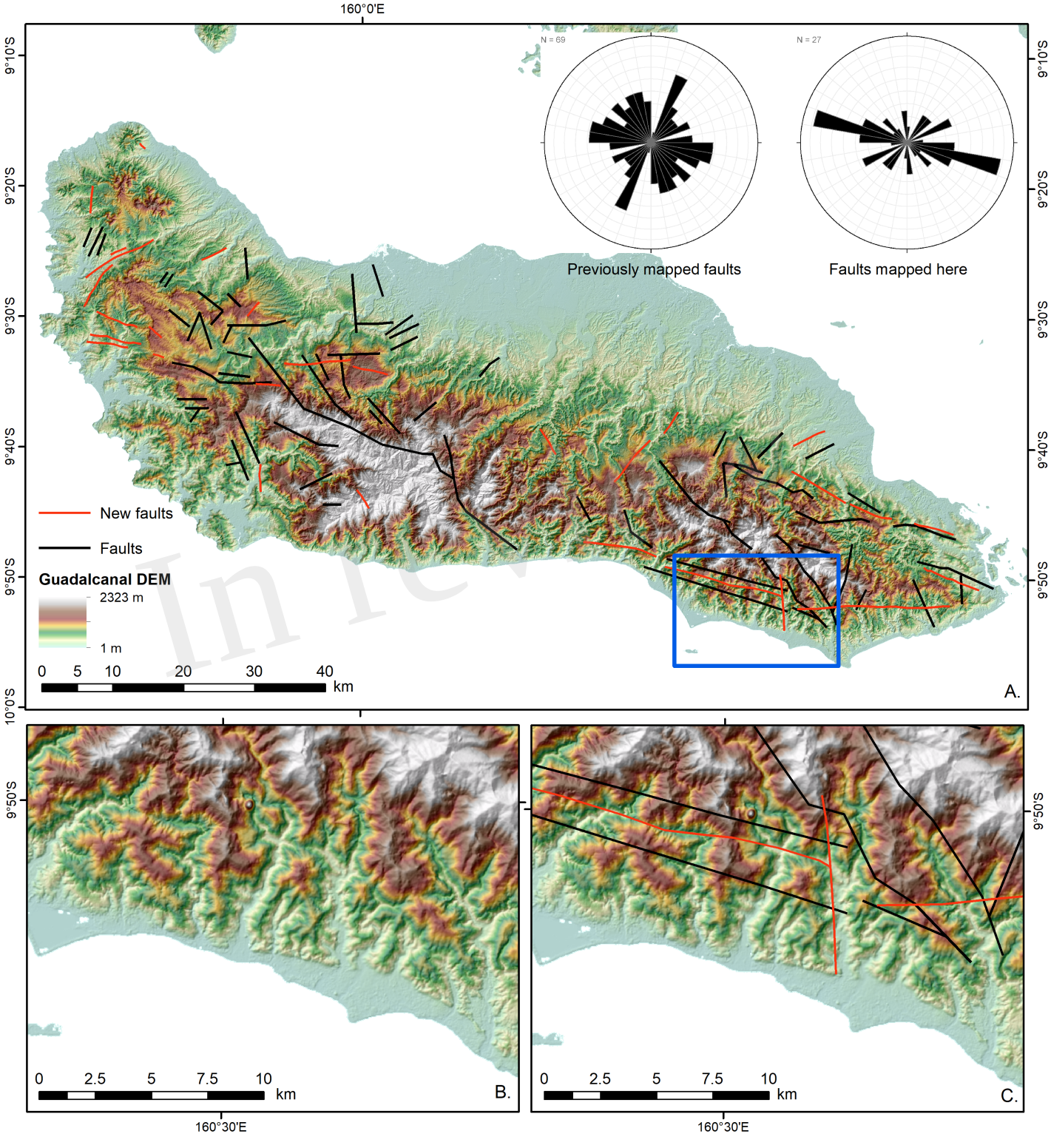
160°0'E
9°10'S
9°20'S
9°30'S
9°40'S
9°50'S
10°0'S
N = 69
N = 27
Previously mapped faults
Faults mapped here
New faults
Faults
Guadalcanal DEM
2323 m
1 m
0 5 10 20 30 40
km
A.
0 2.5 5 7.5 10
km
B.
C.
160°30'E

Figure 5.TIF

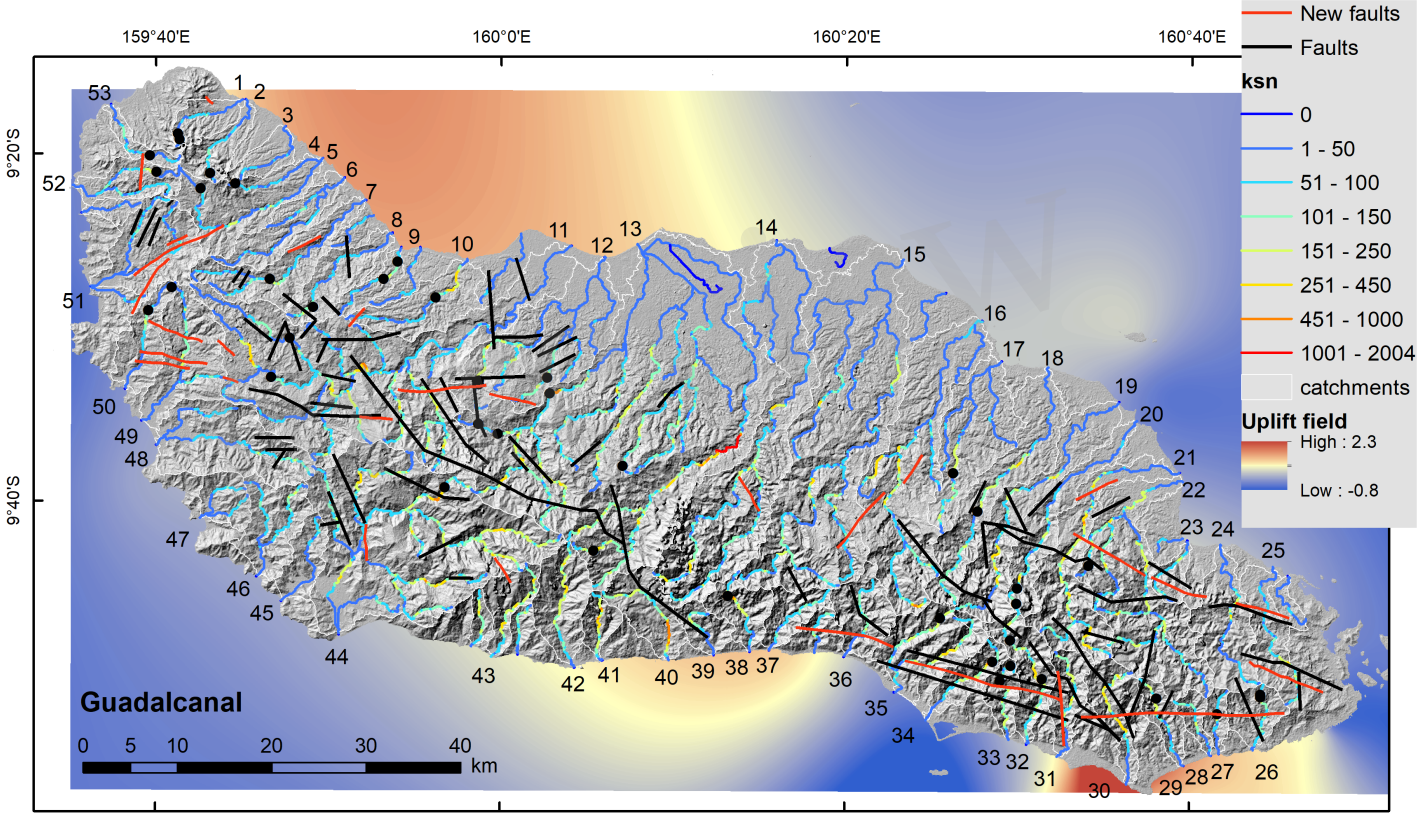
159°40'E
160°0'E
160°20'E
160°40'E
9°20'S
9°40'S
Guadalcanal
0 5 10 20 30 40
km
New faults
Faults
ksn
0
1 - 50
51 - 100
101 - 150
151 - 250
251 - 450
451 - 1000
1001 - 2004
catchments
Uplift field
High : 2.3
Low : -0.8

Figure 6.TIF

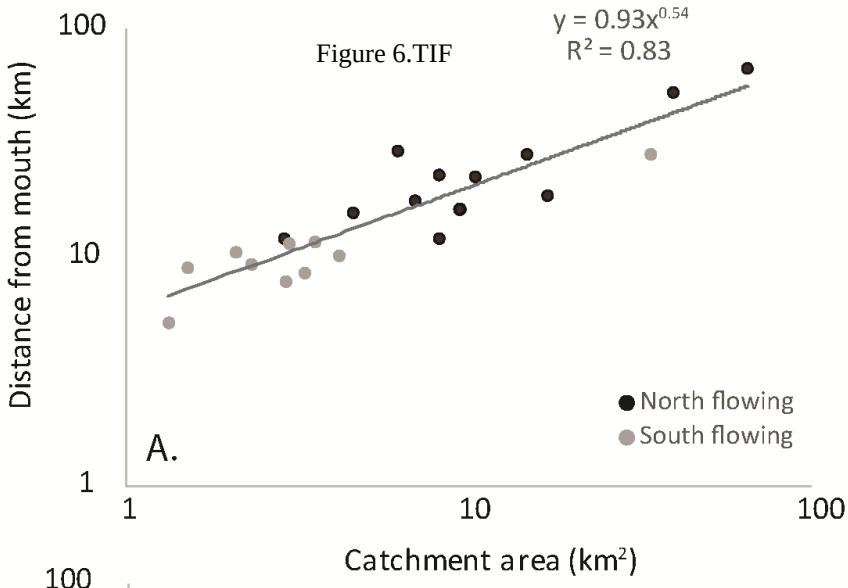

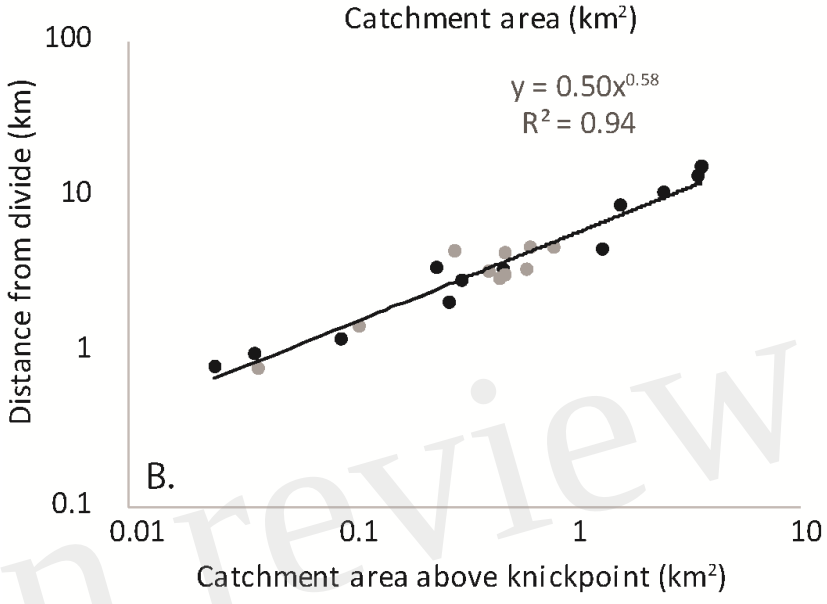

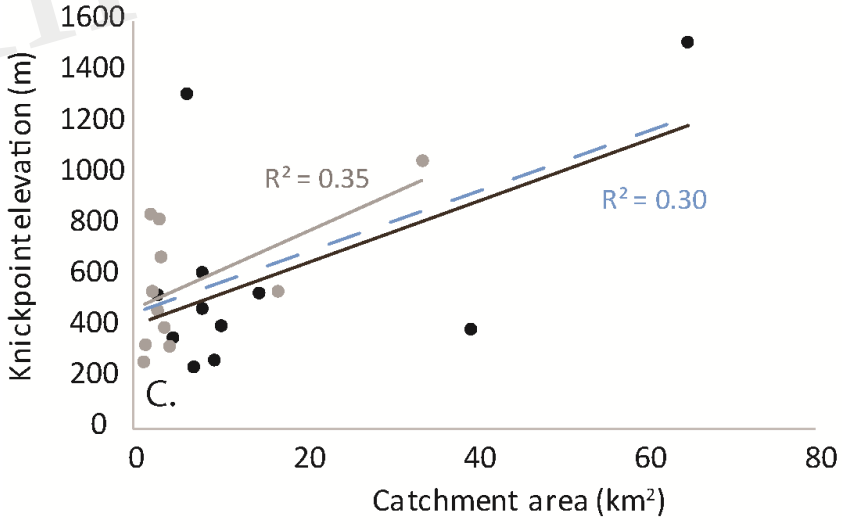

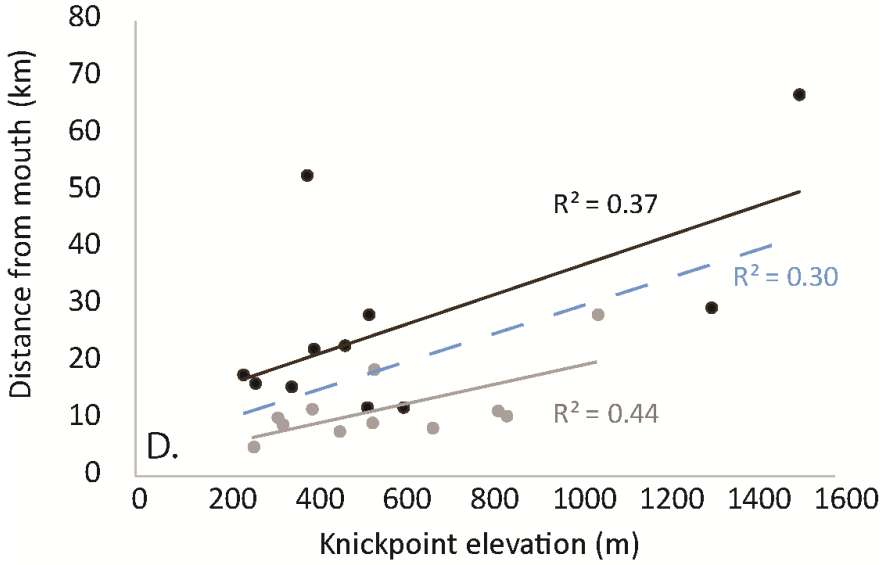

Figure 7.TIF

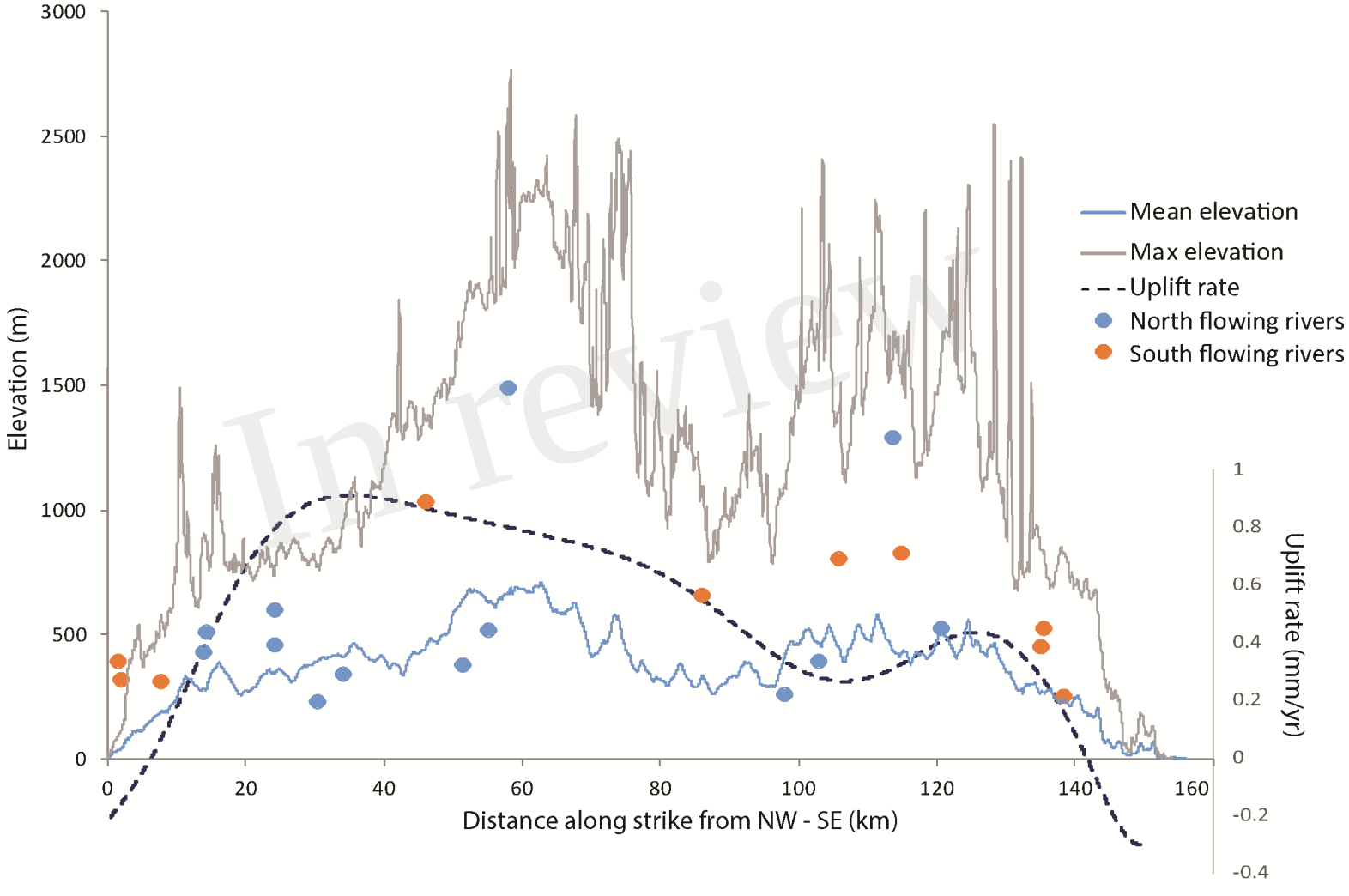

Figure 8.TIF

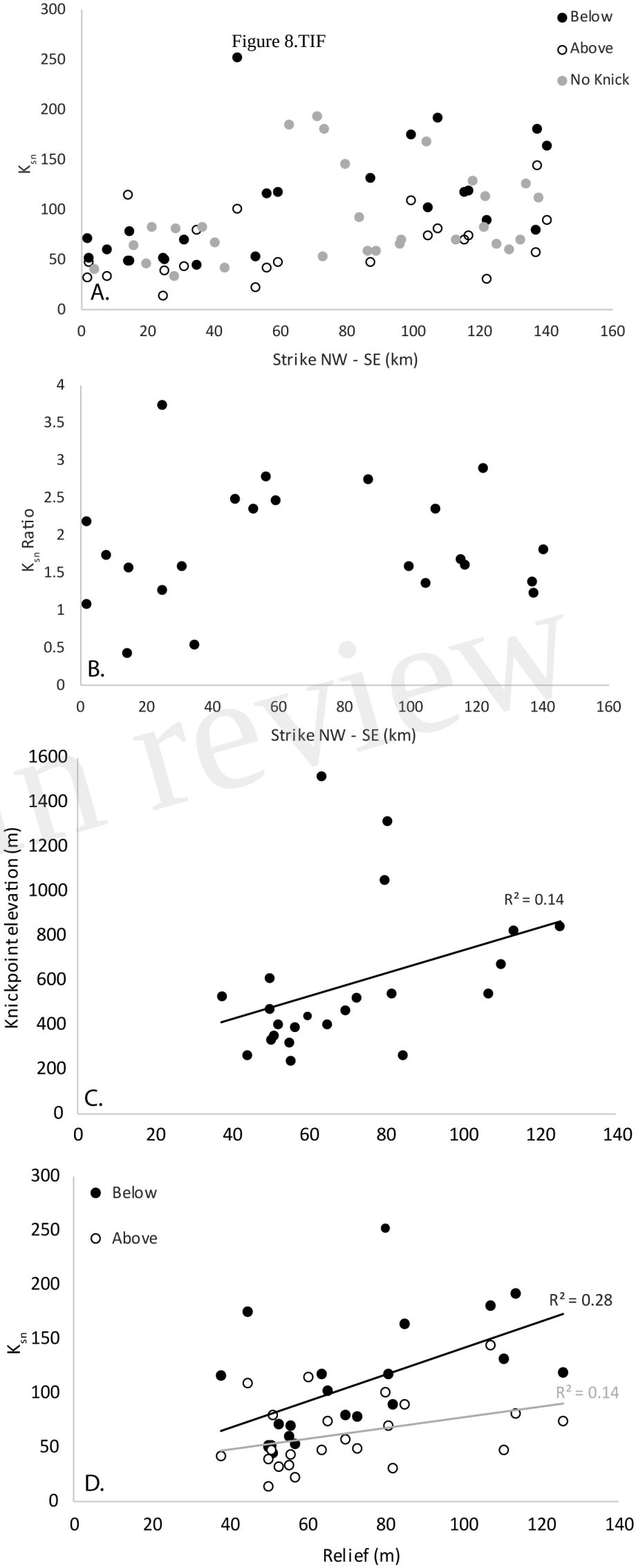

Figure 9.TIF

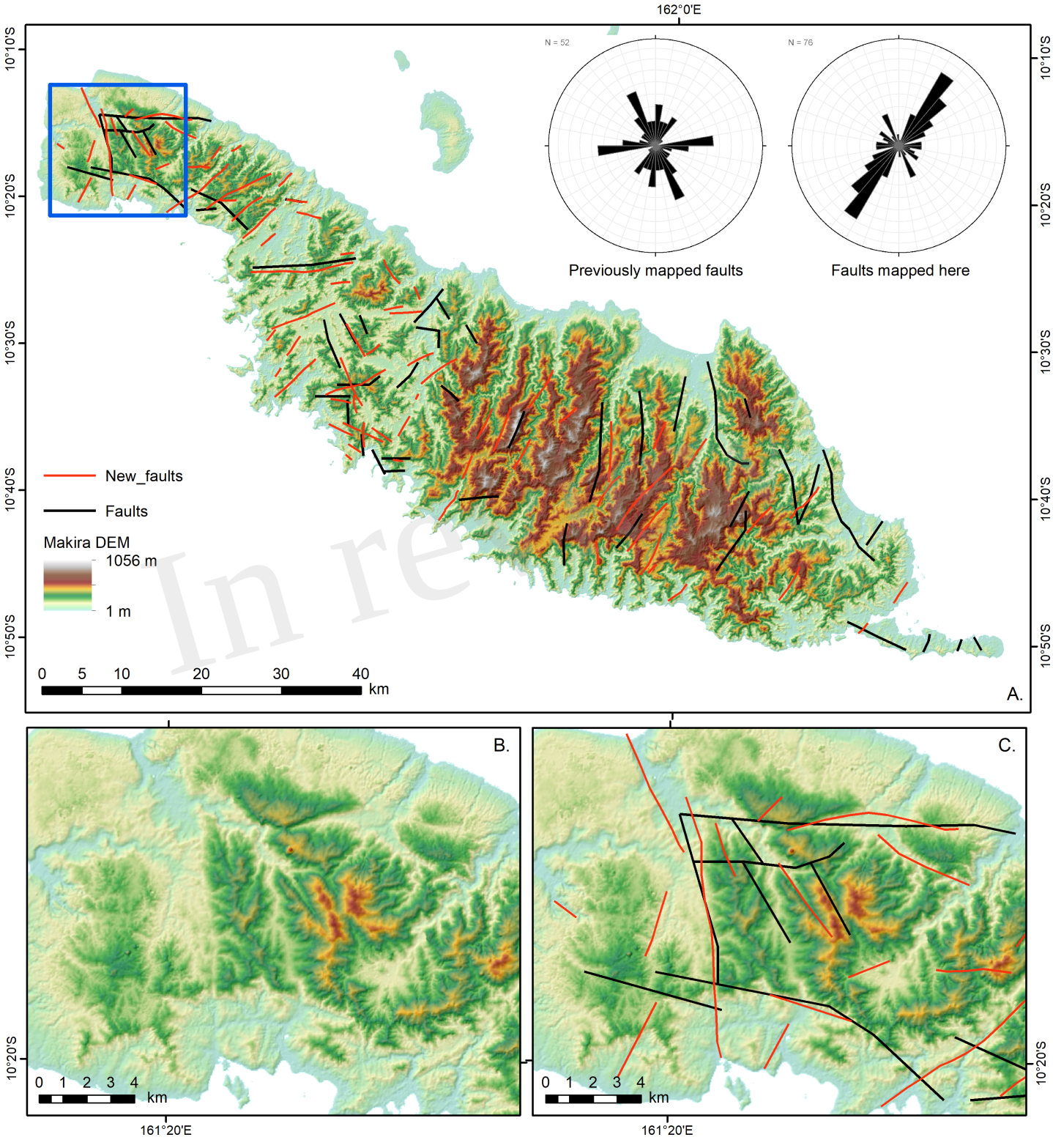
162°0'E
10°10'S
10°20'S
10°30'S
10°40'S
10°50'S
N = 52
N = 76
Previously mapped faults
Faults mapped here
New_faults
Faults
Makira DEM
1056 m
1 m
0 5 10 20 30 40
km
A.
B.
C.
0 1 2 3 4
km
161°20'E

Figure 10.TIF

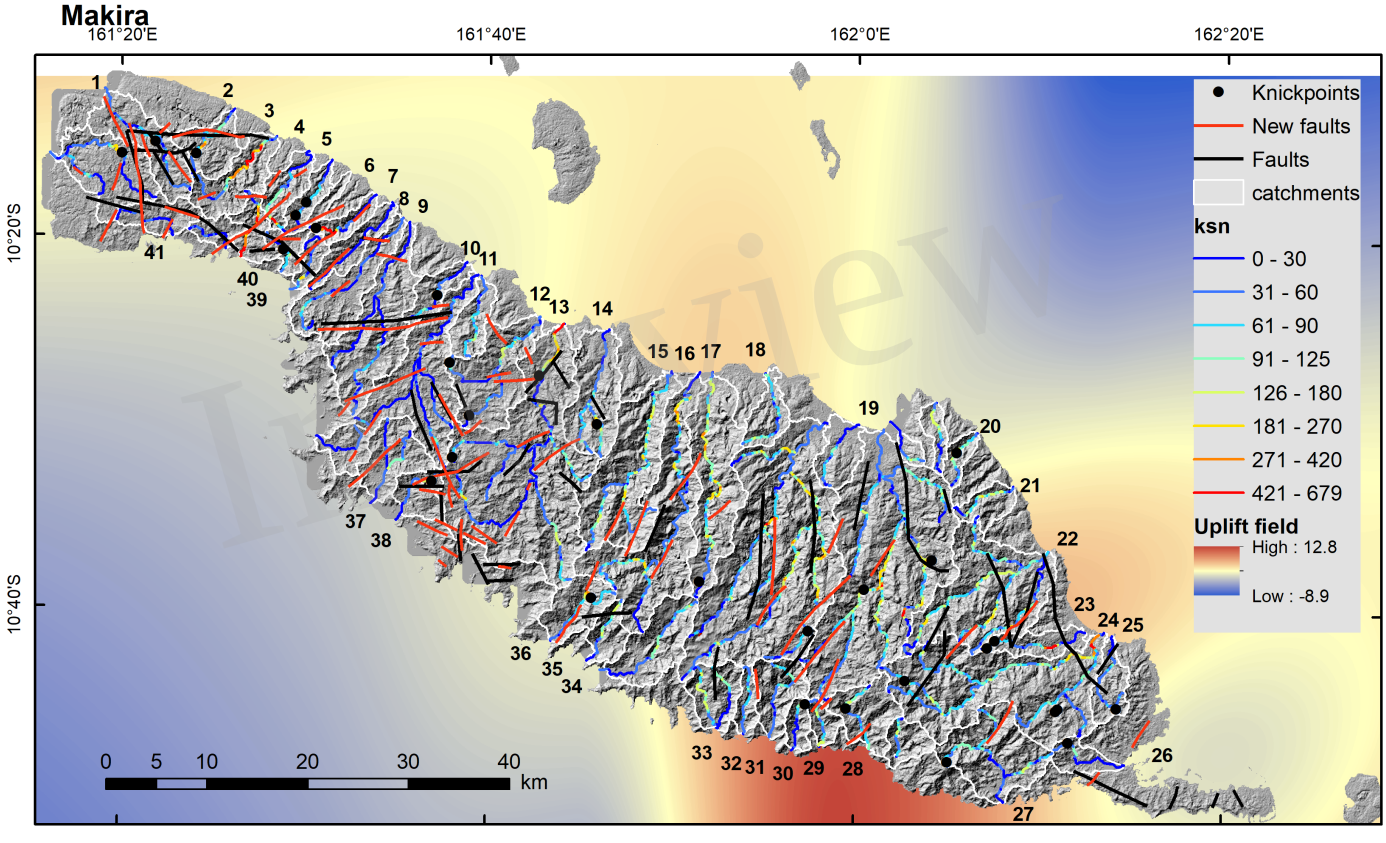

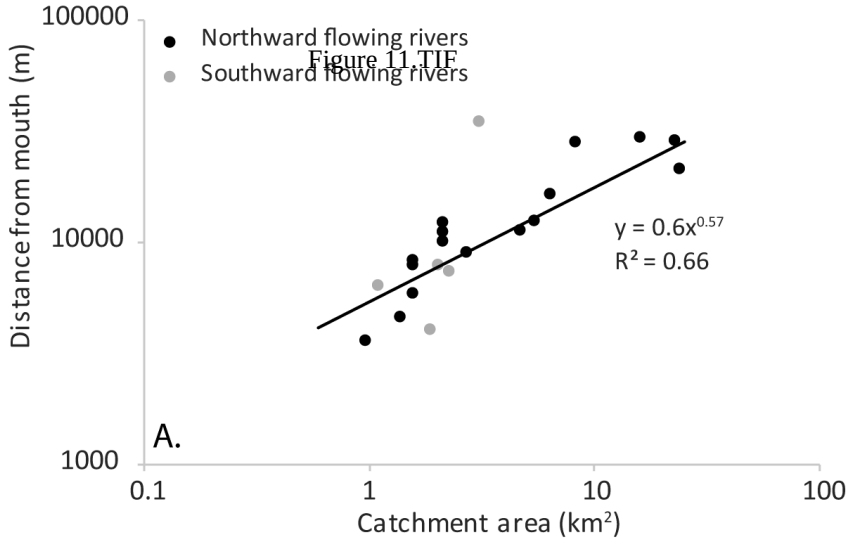

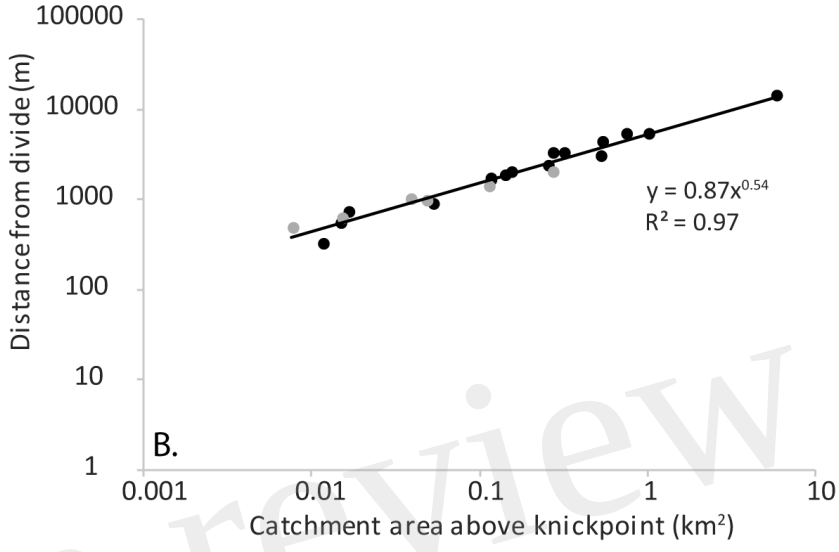

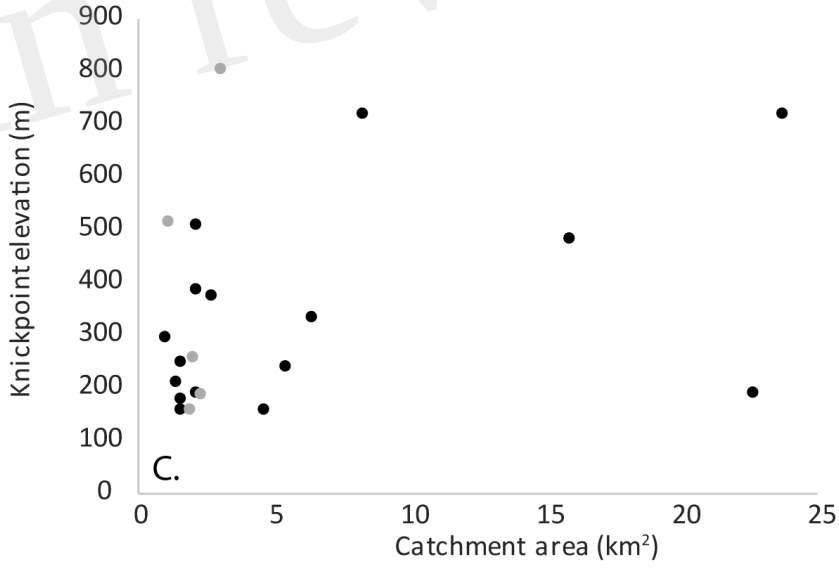

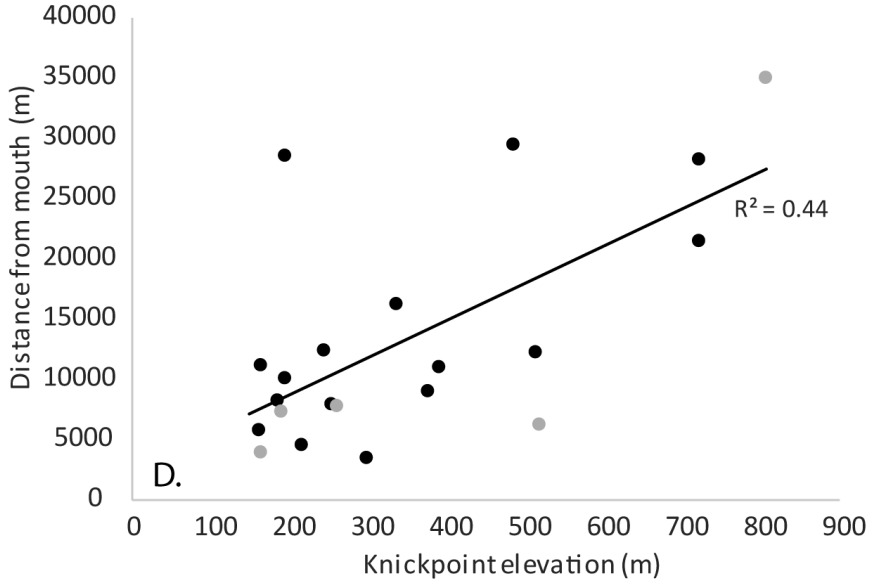

Figure 12.TIF

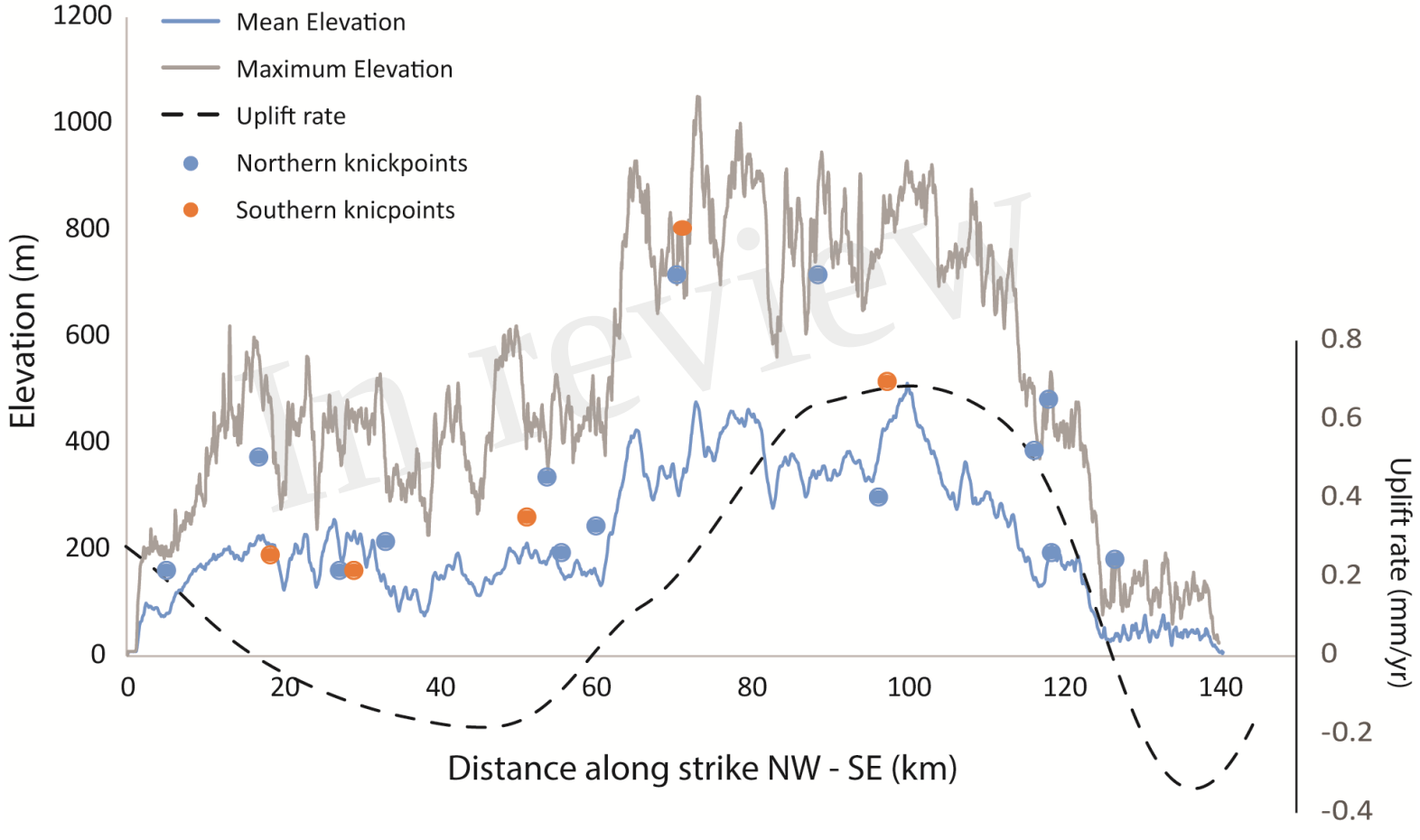

Figure 13.TIF

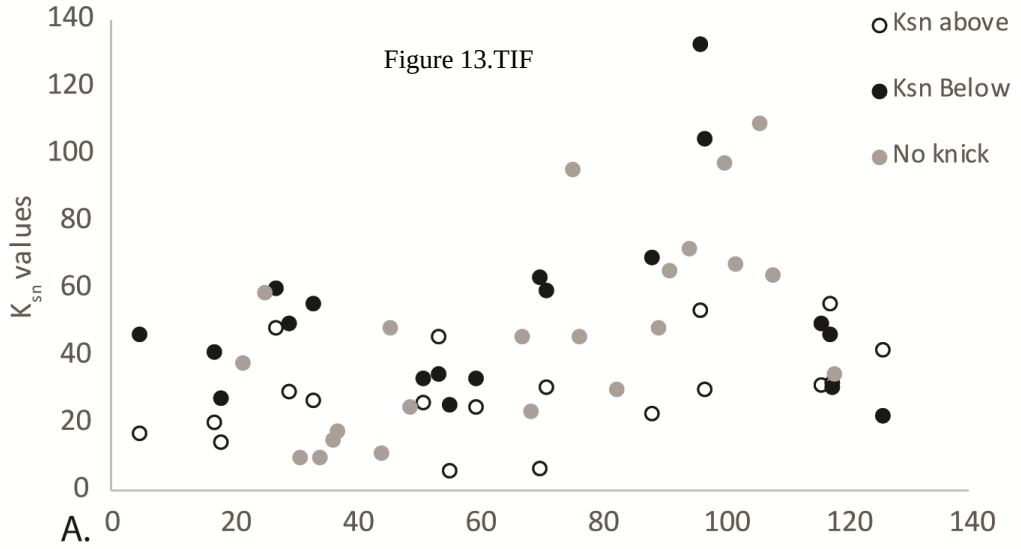

A.

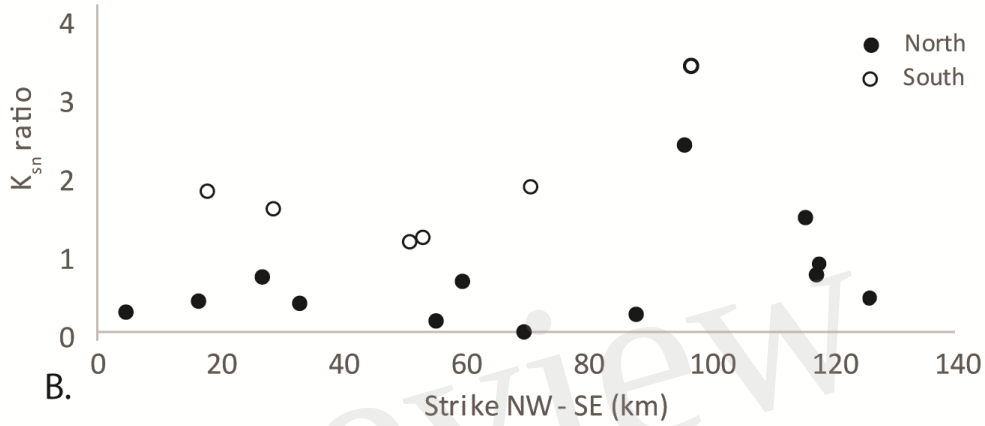

B.

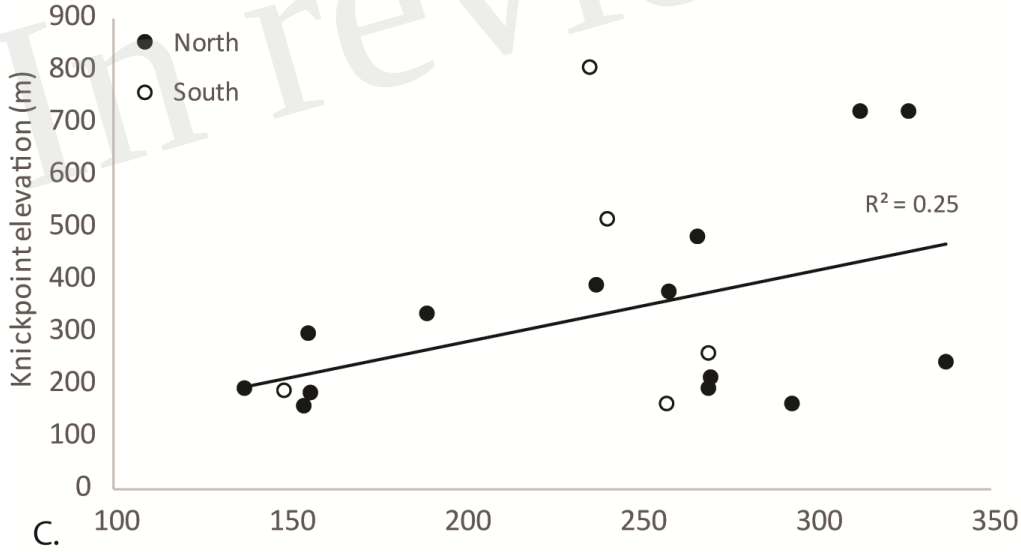

C.

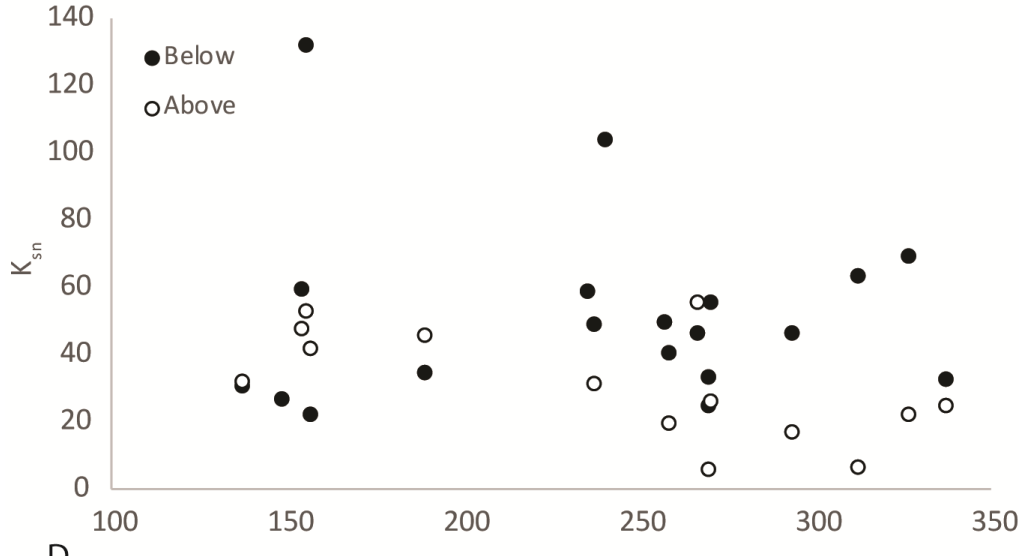

D.

Figure 14.TIF

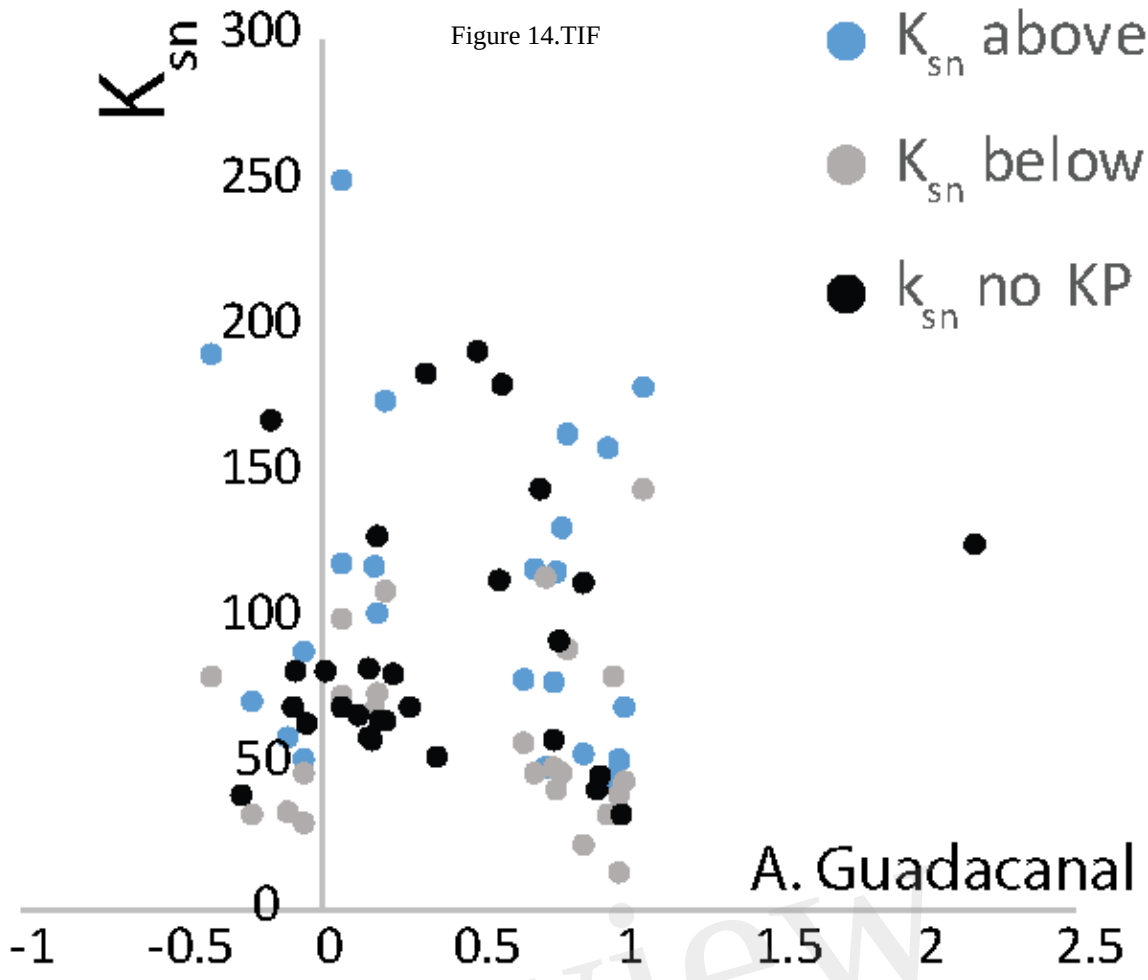

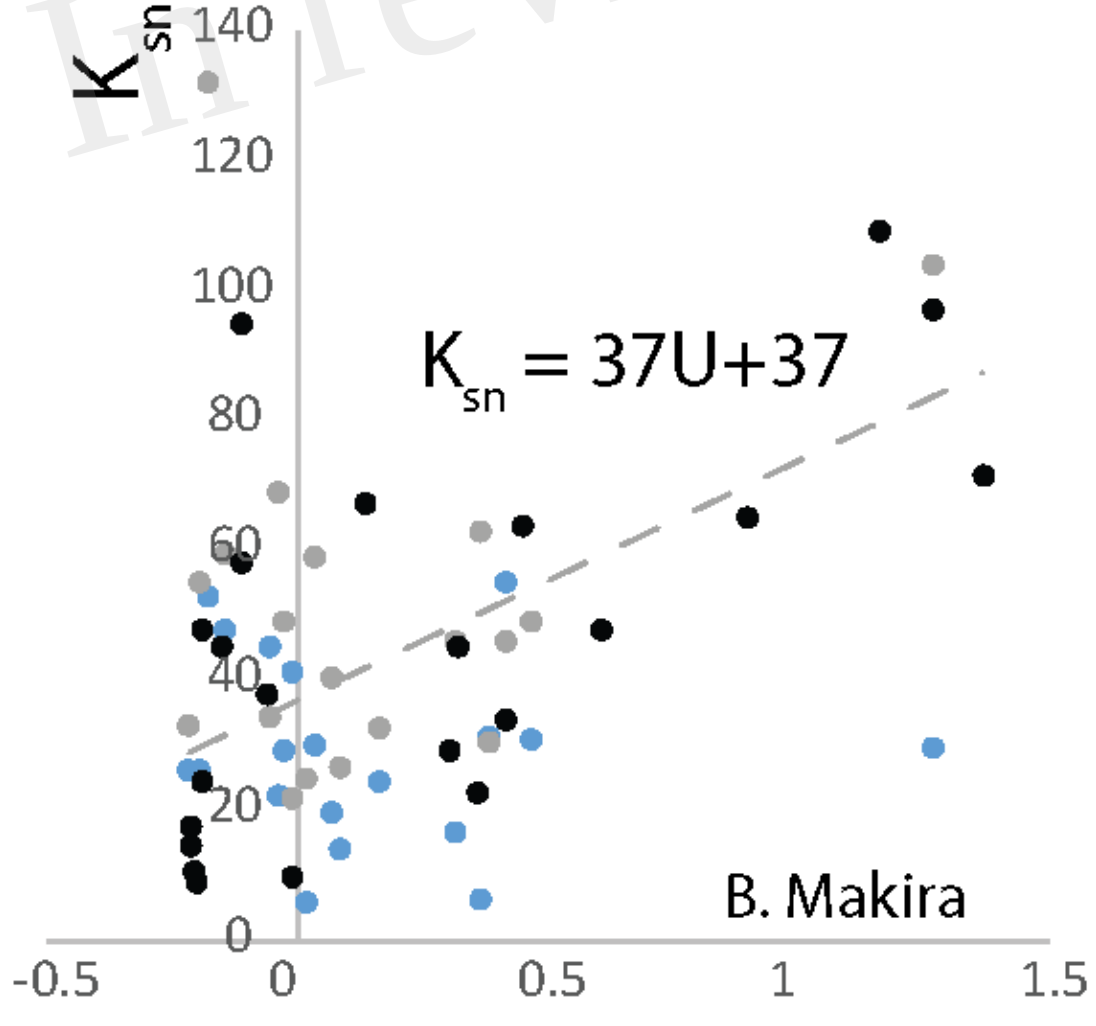

Uplift rate (mm/yr)